2011

Modeling Of Thermal Properties Of Fiber Glass Polyester Resin Composite Under Thermal Degradation Condition

Marvin S. Tsoi
University of Central Florida

MODELING OF THERMAL PROPERTIES OF FIBER GLASS POLYESTER RESIN COMPOSITE UNDER THERMAL DEGRADATION CONDITION

by

MARVIN S. TSOI
B.S.M.E. University of Central Florida, 2008

A thesis submitted in partial fulfillment of the requirements
for the degree of Master in Science in Mechanical Engineering
in the department of Mechanical, Materials and Aerospace Engineering
in the College of Engineering and Computer Science
at the University of Central Florida
Orlando, Florida

Fall Term
2011

ABSTRACT

Composites, though used in a variety of applications from chairs and office supplies to structures of U.S. Navy ships and aircrafts, are not all designed to hold up to extreme heat flux and high temperature. Fiber-reinforced polymeric composites (FRPC) have been proven to provide the much needed physical and mechanical properties under fire exposure. FRPC notable features are its combination of high specific tensile strength, low weight, along with good corrosion and fatigue resistance. However FRPC are susceptible to thermal degradation and decomposition, which yields flammable gas, and are thus highly combustible. This property restricts polymeric material usage.

This study developed a numerical model that simulated the degradation rate and temperature profiles of a fiber-reinforced polyester resin composite exposed to a constant heat flux and hydrocarbon fire in a cone calorimeter. A numerical model is an essential tool because it gives the composite designer the ability to predict results in a time and cost efficient manner. The goal of this thesis is to develop a numerical model to simulate a zonal-layer polyester resin and fiber-glass mat composite and then validate the model with experimental results from a cone calorimeter. By inputting the thermal properties of the layered composite of alternating polymer and polymer-infused glass fiber mat layers, the numerical model is one step closer to representing the experimental data from the cone calorimeter test. The final results are achieved through adding a simulated heat flux from the pilot ignition of the degraded gas of the polyester resin. The results can be coupled into a mechanical model, which may be separately constructed for future study on the mechanical strength of composites under fire conditions.

ACKNOWLEDGEMENTS

I would like to acknowledge my adviser, Dr. Ruey-hung Chen, not only in helping me through this thesis but for helping me understand my own capabilities and improve on my weaknesses. I would like to thank Dr. Jihua Gou and his past and present students and post-doctorate, Dr. Yong Tang, Lee Algozzini, James McKee, Jeremy Lawrence, Jinfeng Zhuge and Fei Liang for helping, teaching and inspiring me on the subject of composites. Thanks to all my friends at Earthrise Space, Inc. for keeping me focused and challenged in all aspects of life. My deepest heartfelt thanks go to my friends, Amy, Josh, Thuy, Nghia for supporting me through graduate school and through difficult times.

TABLE OF CONTENTS

LIST OF FIGURES

LIST OF TABLES

NOMENCLATURE

Symbol	Units	Definition
B	D	Permeability
c_p	$\frac{J}{kg\ K}$	Specific heat of polymer
c_g	$\frac{J}{kg\ K}$	Specific heat of gas from charring
c_c	$\frac{J}{kg\ K}$	Specific heat of char residue
D	m	Sample diameter
h_1	$\frac{W}{m^2K}$	Upper boundary convective coefficient
h_2	$\frac{W}{m^2K}$	Lower boundary convective coefficient
k_c	$\frac{W}{m\ K}$	Thermal Conductivity of char residue
k_p	$\frac{W}{m\ K}$	Thermal Conductivity of polymer
k_g	$\frac{W}{m\ K}$	Thermal Conductivity of gas from charring
k_f	$\frac{W}{m\ K}$	Thermal Conductivity of glass fiber
k_v	$\frac{W}{m\ K}$	Effective thermal conductivity of polymer resin infused fiber-glass mat layer
k_{eff}	$\frac{W}{m\ K}$	Effective thermal conductivity of char layer
l	M	Thickness length
L	$\frac{J}{kg}$	Latent heat of polymer
L_e	m	Mean beam length

N		Number of nodes per zone of numerical model
$\dot{m}''$	$\frac{g}{s\,m^2}$	Mass flux
P	Pa	Pressure
P_a	Pa	Ambient pressure
$\hat{P}$		Dimensionless Pressure
q_0''	$\frac{W}{m^2}$	External radiation heat flux
q_f''	$\frac{W}{m^2}$	Flame radiation heat flux
r		Charring ratio
s	m	Char and polymer interface position
t	s	time
T	K	Local temperature
T_a	K	Ambient Temperature
T_c	K	Critical Temperature
$\hat{T}$		Dimensionless Temperature
v_o	$\frac{m}{s}$	Superficial velocity
V_f		Volume fraction of fiber-glass
x		Landau transformation spatial position
y	m	Spatial position
α_p	$\frac{m^2}{s}$	Thermal diffusivity of polyester resin

α_c	$\frac{m^2}{s}$	Pressure diffusivity of char layer
δ		Dimensionless char and polymer interface position
ε		Material emissivity
ε_f		Flame emissivity
κ	m^{-1}	Extinction coefficient
λ		Diffusivity ratio
σ	$\frac{W}{m^2K^4}$	Stefan-Boltzmann Constant = 5.67×10^{-8}
ρ_c	$\frac{kg}{m^3}$	Density of char residue
$\rho_{g,a}$	$\frac{kg}{m^3}$	Density of gas from charring at ambient temperature
ρ_p	$\frac{kg}{m^3}$	Density of polymer
$\hat{\rho}$		Dimensionless gas density
τ		Dimensionless time

CHAPTER ONE: INTRODUCTION

Composite Laminates

When designing structures, engineers have an obsessive need to make their designs lighter, stronger, faster and better. Driven by this need, the idea of composite laminates was developed. What exactly are composites? A composite laminate is made out of several different materials that retain their own characteristics but work together to make a better defined product. Composites can be found in every day scenarios like the plastic fiberglass chair, fiberglass bathtubs, and many wood products can also be composites with a mixture of waste wood and resin. These materials are popping up everywhere, an example driving factor in the development of composites, specifically natural fiber composites, is the implementation in 2006 by the European Union legislation that 80% vehicles must be reused or recycled, by 2015 this percentage is raised to 85% [1]. Another example is shown in Figure 1, Boeing's 777 and Airbus's A380 are a major source of fiber-reinforced polymer composites [2].

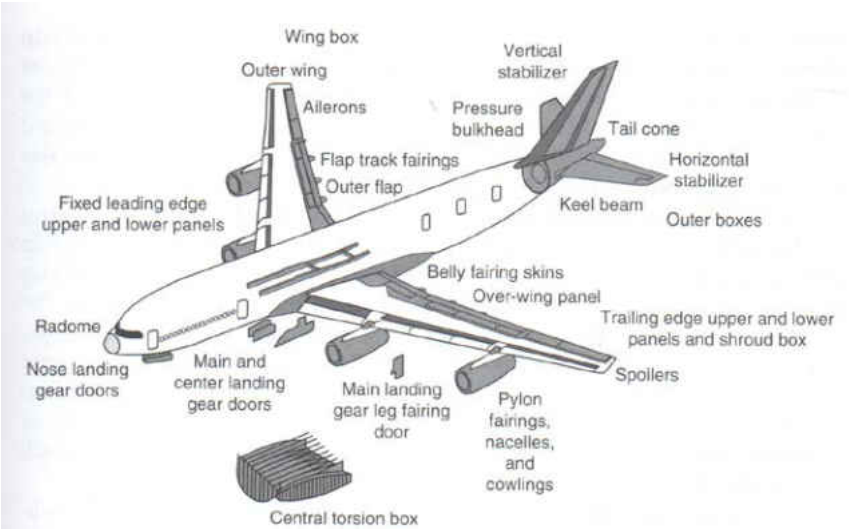

Figure 1: Composite usage on an Airbus A380 taken from reference [2]

Today, engineers have a never before seen ability to customize their material with the usage of composite laminates. Fiber-reinforce composite material consists of any sort of load bearing fibers that are embedded into a matrix of any type, which makes the combination almost endless. Figure 2 demonstrates the basic building blocks of composite design. The fibers provide the majority of the tensile strength characteristic of the overall material; they can be made of glass, carbon, boron, ceramic or natural fibers like hemp or flax. The matrix of the laminate holds the fibers together and provides the major compression characteristics of the overall composite. Common matrix designs are made out of polymer, metal or ceramic. Additives and fiber treatment can be implemented into the fabrication of the composite laminate to improve its properties. It is safe to say that the engineer's imagination is the limit when designing and fabricating composite laminates.

The matrix of the composite can be categorized as ceramic, metallic or polymeric. Ceramic matrices are ideal for their high temperature and thermal shock resistance as well as their high modulus, high hardness, high corrosion resistance and low density. Unfortunately a ceramic matrix is highly brittle and can easily fracture. Metal matrices have an advantage in its long-term resistance to harsh environments, higher yield strength and modulus. However, high density, high melting temperature and the tendency of corrosion at the fiber-matrix interface make the usage of this matrix material a disadvantageous against polymeric matrices [2]. Polymeric matrix composites are the most widely used composite. Yet, they do have limitations in those polymers have a tendency to degrade when subjected to high temperatures and produce highly toxic by-products.

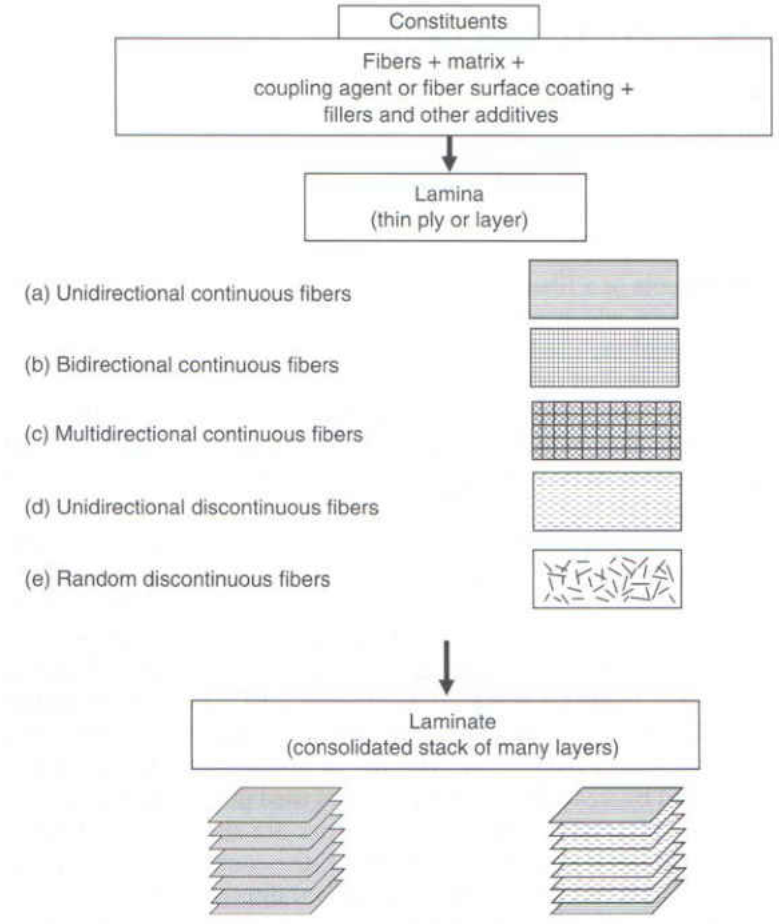

Figure 2: Basic design of a composite laminate taken from reference [2]

Combustion

To understand the variables involved in a degrading and eventually ignited polymer composite, a brief review of combustion phenomena is given. The formation of flames is the process of a self-sustained overall exothermic reaction from a form of gaseous fuel and oxidizer. There are many types of flames, hydrogen, silane, hydrazine, magnesium, hydrocarbon and more. The most common type is a hydrocarbon flame, which means a flame fueled by hydrogen

and carbon molecules. Butane, propane, ethane, methane, and all organic material like polymers are considered to be hydrocarbons, thus creating a hydrocarbon flame if set ablaze.

Flames can be defined into two categories, premixed flames or diffusion flames. A premixed flame is defined when the oxidizer and fuel are mixed at specific quantities before reaching the flame front. Examples are acetylene, propane and butane torches. Diffusion flames are controlled by the diffusion of fuel into the oxidizer until a specific fuel to oxidizer ratio is achieved for the flame. This can be represented by a candle, were the melted candle is the fuel and the surrounding air is the oxidizer. The idea of a diffusion flame can be applied to the characteristic of a burning fiber reinforced polymeric composite (FRPC). However, because the combustion of FRPC is a diffusion flame, the characteristic of this flame will depending highly on the rate of diffusion of the fuel. In this case, it will be the degradation rate of the polymeric material caused by an external source of high heat flux.

An important property that engineers design to know about flames is its temperature and emissivity. By knowing the temperature and heat flux of the hydrocarbon flame, the behavior of flame spread and degradation rate of adjacent polymeric composites can be effectively predicted. There are many variables that affect the flame temperature. One immediate variable is the fuel to oxidizer ratio in a flame, also known as the equivalence ratio. The equivalence ratio, φ, is defined as the fuel to oxidizer ratio of the current flame divided by the fuel to oxidizer ratio if the flame is under stoichiometric condition. The stoichiometric fuel to oxidizer ratio defines a complete reaction were the CO and H_2 molecules are complete consumed, if this is the case for the current flame, then equivalence ratio will equal to 1. This is the most ideal condition thus

producing the highest flame temperature that can be achieved. An equivalence ratio greater than 1 is defined as a fuel-rich flame and a flame with equivalence ratio less than 1 is defined as fuel-lean. As seen in Figure 3, due to the incomplete reaction both case of fuel-rich and fuel-lean reaction produces a lower flame temperature is achieved when compared to the stoichiometric fuel to oxidizer reaction.

Figure 4 shows the structure of a flame is made up of several zones. First zone encountered is the preheat zone, this leads into the reaction zone were the majority of the chemical reaction takes place. The structure of the reaction zone is made up of pyrolysis reaction and a zone where CO and H_2 are consumed. The luminous zone is the part of the reaction zone where the majority of the heat release and reaction takes place [3].

The emissivity of the flame is another parameter that will help predicting the heat flux from a flame. The radiation from a flame is estimated as a translucent medium with self-absorption from soot particles. The self-absorption is a result of soot particles with their own unavoidable radiation absorption coefficient. This result in an effective emissivity related to κ, also known as the absorption or emission coefficient [4]. Unfortunately the absorption coefficient is highly dependent on the soot formation, which is found to be also dependent on the geometry and surrounding environmental conditions of the flame.

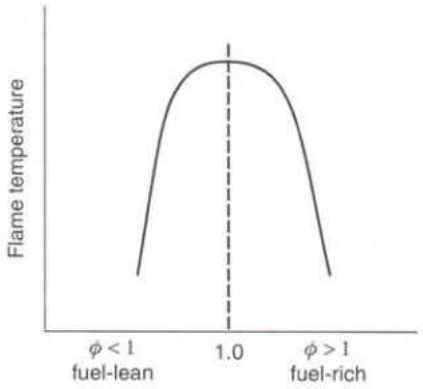

Figure 3: Equivalence ratio effect on flame temperature taken from reference [3]

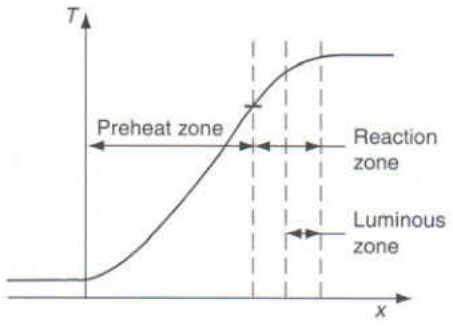

Figure 4: Temperature zone in a laminar flame taken from reference [3]

The usage of polymer in the materials industry is well established but there is still a need for a push on flame retardant research specifically for polymers. Halogen based flame-retardants were the earliest form of fire retardants [5]. This type of retardant is based on the concept of trapping radicals that sustains the combustion process through various chemical reactions to produce a more stable resultant molecule. This limits the amount of self-sustained molecular reactions and eventually the flame decays in strength. Unfortunately in present day the usage of halogen based

flame retardant has been limited due to the significant health and environmental issues its usage has caused.

Another interesting method of flame retardant is the development of intumescent flame retardant. When Intumescent materials are exposed to significant heat, the material will swell and foam up while creating a carbon based char layer. This expanded char layer inhibits heat and mass flux because of its porous structure and results in the protection of the material from further degradation. Unfortunately this method is too costly and not ideal in composites laminates.

The most ideal method of improving the flammability characteristic of a composite is intrinsically improving the polymer properties. By synthesizing polymers with high bonding energy the critical temperature defining its degradation will be increased thus delaying the time it takes for combustion to begin. In order to maximize bonding energy in a polymer it is ideal to make aromatic polymer rings that are resonance stabilized. All bond angles should be perpendicular and should have multiple bonding to several centers and cross-links, as seen in Figure 5, to ensure that there are no bond strains and weakness that may degrade earlier than the rest of the structure. Many fire retardant polymers incorporate aromatic cycles or hetero-cycles for the exact purpose of increasing bonding energy. Kelvar, polyether imides, PEEK and Teflon are notable and most feasible fire retardant polymers that are used widely today and can be incorporated into composites for an added advantage in delaying combustion. These types of polymer structures tend to decompose into char and provide significant protection from high intensity heat flux.

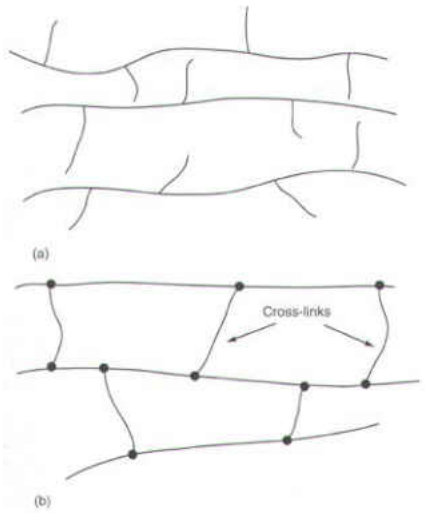

Figure 5: Schematic representation of polymer with (a) no cross-links and (b) cross-links taken from reference [2]

Cone Calorimeter

A cone calorimeter is a measurement apparatus that exposes a user defined material to a focused radiation heater. The applied heat flux can vary between 0 and 100 kW/m^2, in a fire simulation 35 or 50 kW/m2 are widely used. However the applied radiation flux from the heater does not define the total heat flux into the material. Re-radiation, absorptivity of the material and heat flux from ignited flame define the total heat flux into the material.

Cone calorimeters are essential in understanding the parameters of a material's fire properties. The apparatus is capable of measuring parameters like mass loss, heat release rate (HHR), total heat release (THR), smoke production, and carbon-monoxide production. For materials that have a constant effective heat of combustion the rate of mass loss controls the HRR. The same can be said for the total mass loss controlling the THR. Oxygen consumption calorimetry is used

to determine the HRR, different material characteristics can be interpreted from the HRR curve as seen in Figure 6 [6].

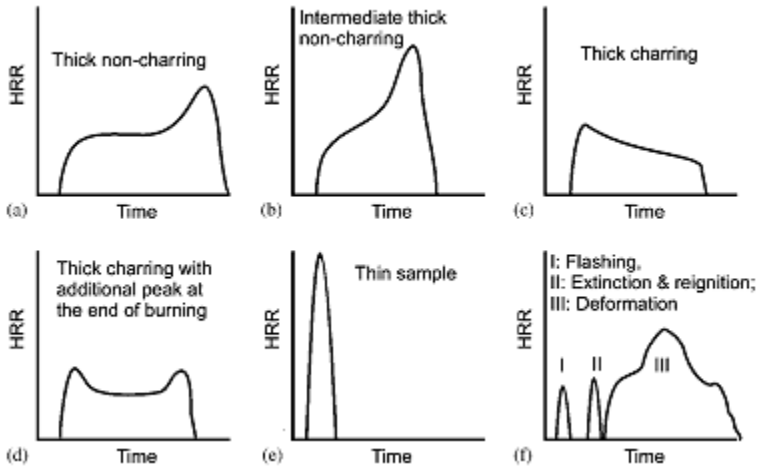

Figure 6: Typical HRR curves taken from reference [6]

Numerical Model

The wide usage of fiber reinforced polymeric composite material mainly as a construction material for buildings, aircrafts and marine structures has prompted the desire for the material to withstand exposure to fire. With these many applications it is necessary to obtain accurate knowledge of the thermal response of polymeric material. Examples of thermal responses are the rate of temperature increase on the front and back surface and within the material and the mass flux of the degrading polymer resulting from the temperature increase.

When polymeric material is exposed to elevated temperature, usually around 200 to 300 °C, they experience a chemical reaction which the polymeric material degrades into gas products and

a form of porous carbon char, the variable *r*, the charring ratio, will be used to define the percentage of char produced while remaining percentage defines the amount of gas produced. This process is called pyrolysis and the porous layer of char residue that is left behind helps protect the rest of the material underneath from exposure to high temperature by creating a layer of low thermal diffusivity about the polymeric material, but because part of the material has degraded to gas, this char layer has no structural strength. As time progresses and temperature increases, the char and polymeric material interface will penetrate further into the material creating a thicker and thicker layer of char as the rest of the polymeric material degrades.

Bamford, Crank and Malan [7], were considered the first to study the degradation of materials, specifically the combustion of wood. They used first order kinetic rate equation and used constant thermal properties in order to create a model. Henderson, Wiebelt and Tant [8], following in Bamford's research, also developed a mathematical model, this time on the degrading polymeric matrices. Henderson's model incorporated the diffusion of the decomposed gases through the char structure, used a n^{th} order kinetic rate (Arrhenius) equation and included the temperature and mass dependent thermal and transport properties. This numerical model proved to be a significant improvement from the model presented by Henderson's predecessor. The material in question by Henderson was a phenol-formaldehyde resin with glass and talc. The numerical model was found to reproduce their experimental data with little deviation in results shown in Figure 7. Figure 7 shows experimental and calculated result of temperature profiles at 0.1, 0.5, 1.0, and 2.9 cm into the depth of the material from the hot surface. The maximum deviation of the numerical calculation to the experimental is no greater than 6%.

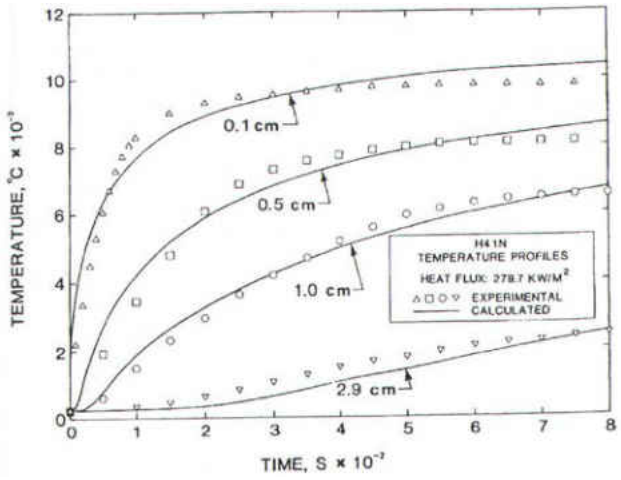

Figure 7: Comparison of calculated and experimental surface temperature taken from reference [8]

Staggs [9] built his numerical model off of the previous research done by Henderson [8] but further explain in detail the derivation of the heat transport governing equations coupled with mass transport through Darcy's law. In this case, the Arrhenius equation was not used in Staggs' derivation of the governing equations, instead the definition of latent heat was used in its place. In the process of deriving the governing equations, the strong assumption that the developed char offers negligible resistance to the flow of gases out and away from the composite structure meaning the pressure gradient along the thickness of the material will be constant in the developing char. With the assumption that there is no resistance to the flow, a superficial velocity can be assumed for Darcy's Law. It is also assumed that the char structure stays intact during the degradation process and not blow off the composite from the mass flux. Figure 8 and 9 displays the hot surface temperature, meaning the surface closest to the heat source, and mass flux results of Staggs' numerical calculation with varying charring ratio, represented by the variable, *r*. [9] Notice that the maximum hot surface temperature is inversely related to the

amount of char produced as seen in Figure 8. The more char produced in the charring process, the lower the hot surface temperature. An obvious conclusion can also be made that the amount of char produced has no effect on the surface temperature before critical charring temperature is reached. The critical temperature is defined as the temperature when charring begins for a material, in Staggs' case, this temperature is defined as 600 K. Figure 9 shows the results of the mass flux from various charring ratio; it is reasonable to see a shorter time to total degradation and a lower mass flux as the charring ratio increases.

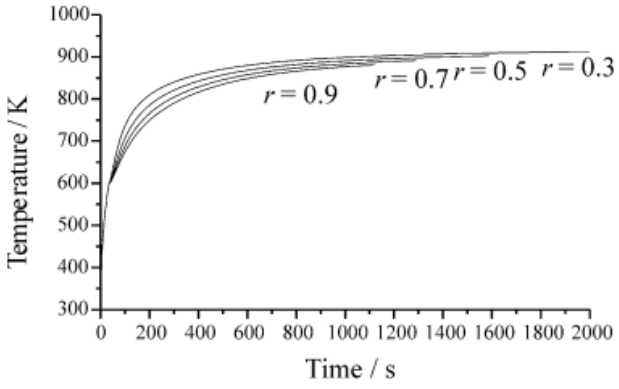

Figure 8: Comparison of calculated hot surface temperature taken from reference [9]

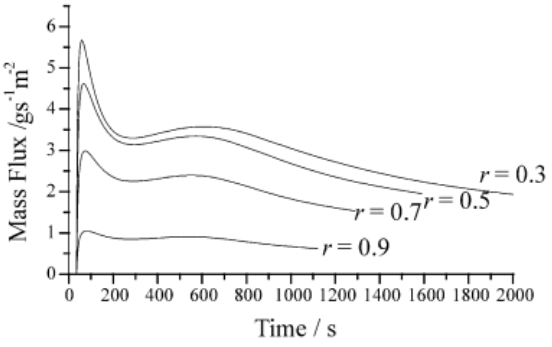

Figure 9: Comparison of calculated mass flux taken from reference [9]

Combustion

Quintiere [11] provides an in depth review on the theoretical basis for flammability properties of a material. An important example of these properties is the burning rate per unit area with convection and flame radiation boundary conditions. By interpreting experimental data, many essential parameters in understanding the flammability properties of certain material can be found. It is show that material properties play a significant role in the ignition, rate of burning per area, energy release rate and flame spread characteristic of the material.

Radiant heating is an important factor in the burning and fire growth on a material. This heat flux can come from any sources like a nearby heater, heated surface, fire or smoke. Flame radiation can be represented by a homogeneous translucent medium of grey gas flame with a mean beam length and an extinction/absorption coefficient [11]. In a cone calorimeter where the sample is oriented horizontally and the flame height is larger than the sample diameter, the mean beam length can be estimated as 0.65 times the sample diameter [10].

In Jiang's paper [12], the importance of fire ventilation on flame emissivity was examined. If the flame is under-ventilated, meaning a less than 0 equivalence ratio, then the excess soot will cause the flame radiation and temperature to be highly dependent on the ventilation. If the equivalence ratio is at the other extreme, $\varphi > 1$, for a well-ventilated then the heat flux and temperature of the flame is independent of ventilation. The presence of soot particles strongly affects the emissivity of the flame. In order to calculate the heat flux of a flame, the amount of soot needs to be known to calculate the self-absorption effect on the total emissivity of the flame

[12]. Brian T. Rhodes [13] analyses PMMA in a cone calorimeter assembly and found that the emissivity of the flame is approximately constant at 0.09, giving an extinction coefficient of about 1.4 m^{-1} [13]. But the size and amount of soot affect the extinction coefficient. The more soot a flame produces the higher the extinction coefficient and thus increases the amount of heat flux produced by the flame.

CHAPTER TWO: METHODOLOGY

Homogeneous single layer material

The physics of degrading polymeric material is presented in order to effectively produce a numerical model for simulation. This one-dimensional homogeneous single layer model closely represents Staggs' simulation that was presented [9]. Figure 10 shows the schematic of the degrading polymer. The top boundary is exposed to a radiant heat flux and convective heat transfer. An issue with this model is knowing when the material begins to degrade, producing char and combustible vapor. The critical temperature, T_c, was used as the criteria to define the conditions for charring, although in real conditions, this is not the case.

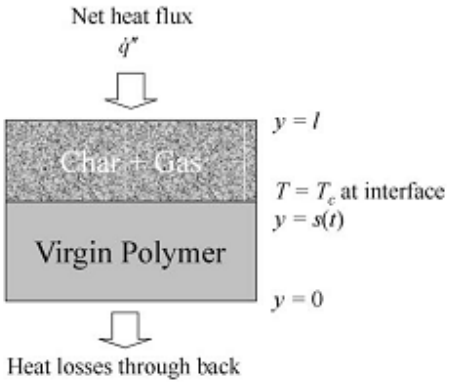

Figure 10: Schematic of degrading polymer taken from reference [9]

The char layer plays a significant role in fire-retardant because of its porous structure. As the virgin polymer degrades, a fraction, defined in this simulation as *r*, of polymer is turned into char while the rest, *1-r*, is degraded into gas and flows upwards and out of the char structure. This porous char structure provides a thermal insulation because of its significantly lower effective

thermal conductivity, k_{eff}. It is estimated that the k_{eff} of the char and gas structure is bounded within a range given as [15]

$$\frac{r\frac{k_g}{k_c}}{(1-r)+r\frac{k_g}{k_c}} \leq \frac{k_{eff}-k_g}{k_c-k_g} \leq r. \tag{1}$$

For the purpose of this analysis, a bold assumption that the thermal conductivity will be atht e upper range of Equation (1) and that the properties of char are the same as the properties of the polymer, where $k_c = k_p$ and $\rho_c = \rho_p$ is used and the gas generated by the charring process has similar properties as air.

The governing equation for the physics within the charring layer is

$$\left((1-r)\rho_g c_g + r\rho_c c_c\right)\frac{d\hat{T}}{dt} + \rho_g c_g v_o \frac{d\hat{T}}{dy} = \frac{\partial}{\partial y}\left(k_{eff}\frac{d\hat{T}}{dy}\right) \tag{2}$$

and the equation for solid virgin polymer with no charring is given as

$$\frac{d\hat{T}}{dt} = \alpha_p \frac{\partial^2 \hat{T}}{\partial y^2}. \tag{3}$$

Where $\alpha_p = \frac{k_p}{\rho_p c_p}$, dimensionless Temperature is defined as $\hat{T} = \frac{T}{T_a}$. The energy loss from the gas flowing through the charred layer and out of the material is expressed in the 2nd term of Equation (2). In order to solve the superficial velocity term, the Darcy expression,

$$\overrightarrow{v_o} = -\frac{B}{\mu}\nabla P, \tag{4}$$

and mass conservation for the exiting gas,

$$(1-r)\left(\frac{d\rho_g}{dt}\right)+\nabla.\left(\rho_g\overrightarrow{v_o}\right)=0, \tag{5}$$

are utilized. Darcy's expression, conservation of mass for the gas and ideal gas law are combined together to create

$$\frac{\partial}{\partial t}\left(\frac{\hat{P}}{\hat{T}}\right)=\frac{BP_a}{(1-r)\mu}\nabla.\left(\frac{\hat{P}}{\hat{T}}\nabla\hat{P}\right). \tag{6}$$

Where $\hat{P}=\frac{P}{P_a}$ and $\alpha_c=\frac{BP_a}{(1-r)\mu}$ are the definitions of dimensionless pressure and pressure diffusivity, respectively.

The surface or top boundary condition is defined as

$$\frac{\varepsilon\dot{q}_0^{"}}{T_a}+h_1\left(1-\hat{T}\right)+\varepsilon\sigma T_a^3\left(1-\hat{T}^4\right)-\rho_g c_g v_o\frac{d\hat{T}}{dy}+k_{eff}\frac{d\hat{T}}{dy}=\left((1-r)\rho_g c_g+r\rho_p c_p\right)\frac{d\hat{T}}{dt}, \tag{7}$$

which takes into account the external heat flux from the heater, convective heat transfer and re-radiation from the material. The char and polymer interface was fixed at a constant temperature at the defined critical temperature. The boundary condition of the backside, or bottom, is governed by only convective heat transfer,

$$-k_p\frac{d\hat{T}}{dy}+h_2\left(1-\hat{T}\right)=\rho_p c_p\frac{d\hat{T}}{dt}. \tag{8}$$

In order to simplify the numerical model, a Landau transformation [16] is used and all variables are non-dimensionalized with $\tau = \frac{\alpha_p}{l^2} t$, for dimensionless time, $\delta = 1 - \frac{s(t)}{l}$ for dimensionless char and polymer interface positions and diffusivity ratio, $\lambda = \frac{\alpha_c}{\alpha_p}$.

$$x = \frac{y - s(t)}{l - s(t)}, \; s(t) < y \leq l, \tag{9}$$

$$x = \frac{y - s(t)}{s(t)}, \; 0 \leq y < s(t), \tag{10}$$

describes the Landau transformation. The coordinate transformation will be beneficial because the char and polymer interface will always be at x = 0 while the top and bottom surface will be x = 1 and x = -1 respectively.

By applying the non-dimensionalization to the coupled Darcy's and continuity equation,

$$\delta^2 \frac{\partial}{\partial \tau}\left(\frac{\hat{P}}{\hat{T}}\right) + (1 - x)\delta \frac{d\delta}{d\tau}\frac{\partial}{\partial x}\left(\frac{\hat{P}}{\hat{T}}\right) = \lambda \frac{\partial}{\partial x}\left(\frac{\hat{P}}{\hat{T}}\frac{\partial \hat{P}}{\partial x}\right) \tag{11}$$

is achieved. A typical value for the pressure diffusivity, α_c, is in the order of 0.001 m^2/s, and typical thermal diffusivity of polymer resin, α_p, is approximately 1.33e-7 W/m-K. Thus the diffusivity ratio, λ, can be reasoned to be of a significantly large number. In order to prevent the pressure gradient from diverging to an unreasonable number, from Equation (11), the right hand side of should equal to zero, as seen in

$$\frac{\partial}{\partial x}\left(\frac{\hat{P}}{\hat{T}}\frac{\partial \hat{P}}{\partial x}\right) = 0. \tag{12}$$

This equation dictates the pressure gradient within the charring layer. By integrating this term the dimensionless pressure is

$$\hat{P} \approx 1 + \frac{\rho_p}{\lambda \rho_{g,a}} \delta \frac{d\delta}{d\tau} \int_x^1 \hat{T} dx. \tag{13}$$

By combining Equation (2) with Equation (4) and using the redefined dimensionless mass flux,

$$-\hat{\rho}_g \frac{\partial \hat{P}}{\partial x} \approx \frac{\rho_p}{\lambda \rho_{g,a}} \delta \frac{d\delta}{d\tau}, \tag{14}$$

along with the definition of dimensionless density, $\hat{\rho}_g = \frac{\rho_g}{\rho_{g,a}} = \frac{\hat{P}}{\hat{T}}$ the final equation for the charring layer is

$$\left((1-r)\frac{\rho_{g,a} c_g}{\rho_p c_p}\hat{\rho}_g + r\right)\left(\delta^2 \frac{\partial \hat{T}}{\partial \tau} + (1-x)\delta \frac{d\delta}{d\tau}\frac{\partial \hat{T}}{\partial x}\right) + (1-r)\left(\frac{c_g}{c_p}\right)\delta \frac{d\delta}{d\tau}\frac{\partial \hat{T}}{\partial x} =$$

$$\left((1-r)\left(\frac{k_g}{k_p}\right) + r\right)\frac{\partial^2 \hat{T}}{\partial x^2}. \tag{15}$$

While the dimensionless equation for the layer with no presence of char and only polymer is expressed using

$$\frac{\partial \hat{T}}{\partial \tau} + \frac{(1+x)}{(1-\delta)}\frac{d\delta}{d\tau}\frac{\partial \hat{T}}{\partial x} = \frac{1}{(1-\delta)^2}\frac{\partial \hat{T}^2}{\partial^2 x}. \tag{16}$$

The top boundary layer with an imposed radiation heat flux is

$$\frac{\varepsilon q_0^{"}}{T_a} + h_1\left(1-\hat{T}\right) + \varepsilon\sigma T_a^3\left(1-\hat{T}^4\right) + \frac{k_{eff}}{l\,\delta}\frac{\partial\hat{T}}{\partial x} + \frac{c_g k_p}{c_p\, l}(1-r)\frac{d\delta}{d\tau}dx =$$

$$\frac{k_p}{l}\delta\frac{dx}{2}\frac{\partial\hat{T}}{\partial\tau} \tag{17}$$

and for the lower boundary layer with only convective heat transfer is

$$\frac{k_p}{l(1-\delta)}\frac{\partial\hat{T}}{\partial x} + h_2\left(1-\hat{T}\right) = \frac{(1-\delta)}{2}\left(\frac{k_p}{l}\right)\left(\frac{\partial\hat{T}}{\partial\tau} + \frac{1-x}{\delta}\frac{d\delta}{d\tau}\frac{\partial\hat{T}}{\partial x}\right). \tag{18}$$

In order to solve the system of equations defined by the presented governing equation, a few variable definitions are absent. The variable for the dimensionless charring rate $\frac{d\delta}{d\tau}$ can be found by conservation of energy at the char and polymer interface. Latent heat of gasification of the polymer is taken into consideration in

$$k_{eff}\left.\frac{d\hat{T}}{dy}\right|_{y=s+} - k_p\left.\frac{d\hat{T}}{dy}\right|_{y=s-} = -\frac{\rho_p L}{T_a}\frac{ds}{dt} \tag{19}$$

to define the rate of polymer degradation. Solving for $\frac{d\delta}{d\tau}$ is an iterative process where a reasonable $\frac{d\delta}{d\tau}$ is first assumed, then the governing equations are solved. The resulting temperature profile is then used in solving the left hand side of Equation (19). The right hand side is solved using the material properties and the assumed $\frac{d\delta}{d\tau}$ and then compared to the left hand side of the equation. A new assumption of $\frac{d\delta}{d\tau}$ is then made until Equation (19) is satisfied.

After finding the $\frac{d\delta}{d\tau}$, δ for the next time step is found by integration. $\frac{d\delta}{d\tau}$ can then be converted to mass flux with the units of $\frac{g}{s\,m^2}$ by

$$\dot{m}'' = (1000)\frac{\alpha_p}{l}(\rho_p - \rho_g)(1 - r)\frac{d\delta}{d\tau}. \tag{20}$$

At time is at 0 second, the model is composed of only virgin polyester resin with no charring. When exposed to a heat flux, the surface temperature rises. In this model, charring will not start until the critical temperature is reached. Right when the critical temperature is reached, the system of governing equations is modified to satisfy the charring and degrading layer. The model is solved until the char and polymer interface reaches the bottom of the material.

The zonal model is developed exactly the same as the single homogeneous layer model discussed in the previous section, the only difference lie in the amount of nodes and the change in material property as seen in Figure 14. When incorporating the glass fiber mats,

$$\frac{k_v}{k_p} = 1 + \frac{2V_f}{\left(\frac{k_p + k_f}{k_f - k_p}\right) - V_f + \left(\frac{k_p - k_f}{k_p + k_f}\right)\left(0.3058V_f^4\right)} \tag{21}$$

is used to calculate the effective thermal conductivity of a layer with glass fiber mat and polyester resin, k_v, with no charring [10]. Where V_f is the volume fraction of only the glass fiber and polymer layer, k_p and k_f are the individual through thickness thermal conductivity of polymer resin and fiber glass mat respectively.

The addition of a hydrocarbon flame to the numerical model can be beneficial in the analysis because the combustible gas from the degrading polymer can ignite. Radiation heat flux from a flame is

$$q_f^{"} = \varepsilon_f \sigma \left({T_f}^4 - {T_s}^4 \right), \tag{22}$$

where ε_f is the emissivity of the flame, T_f is the flame temperature and T_s is the composite's surface temperature.

$$\varepsilon_f = 1 - e^{(-\kappa L_e)} \tag{23}$$

defines the emissivity of a translucent medium, in this case, of the combustion gas in the flame. The extinction coefficient, κ, and the mean beam length,

$$L_e = 0.65D, \tag{24}$$

is needed to solve for the total heat flux from the flame in Equation (19). Even though the flame temperature is highly dependent on many variables, it can be assumed that under a cone calorimeter experiment, the flame temperature is around 1300 K to 1600 K.

Figure 11 represents the spatial discretization along the thickness of the material of virgin polymer, while Figure 12 represents the discretization of a charring model and Figure 13 represent the zonal-layer model for multiple material which will be used to model a glass fiber reinforced polyester resin composite. The positions of the nodes are spaced equally throughout the char layer or polymer layer, but not spaced evenly through the overall material as seen in Figure 12. A node will coincide with each boundary. The nodes are assigned governing

equations in implicit backwards difference style. After assembling the set of governing equations, the fsolve function in MATLAB is used to solve them at constant time step interval of 0.1 second. This function uses the Levenberg-Marquardt algorithm with convergence criteria of 10^{-5} K to solve the finite difference problem. The mass flux and top, middle and bottom temperatures are all recorded and used for experimental comparison.

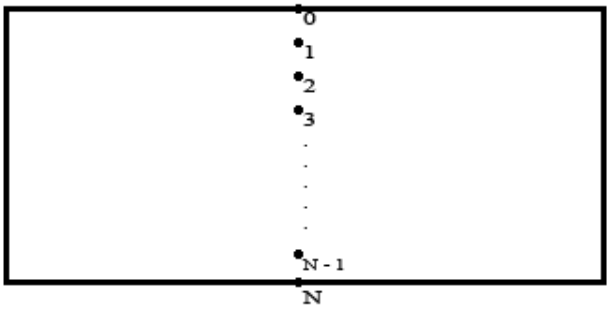

Figure 11: Discretization of single-layer homogeneous polymer model prior to degradation

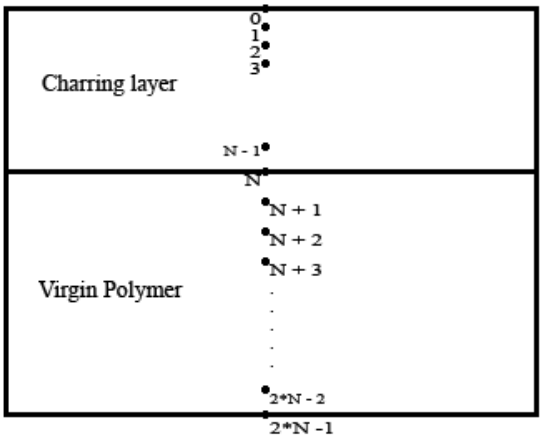

Figure 12: Discretization of single-layer homogeneous polymer model during degradation

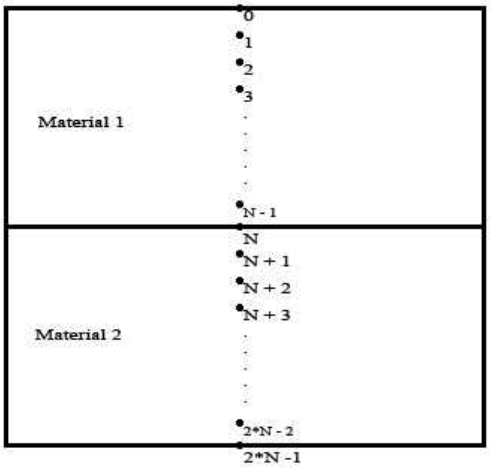

Figure 13: Discretization of zonal-layer model prior to degradation

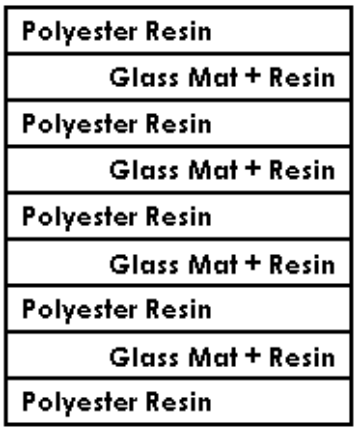

Figure 14: Zonal-layer model schematic

CHAPTER THREE: RESULTS AND DISCUSSION

Homogeneous single layer material

In order to validate the methodology for the presented numerical model, the results are compared to known literature. This numerical model was developed from the same methodology as Staggs' model, therefore Staggs' results were used as a validation criteria. Staggs models a single layer homogeneous polymeric material, Table 1, with an overall thickness of 10 mm, exposed to a constant radiation heat source. Other than the defined external heat flux, the upper boundary of the material will re-radiate energy and the gas flow out of the material from the charring process will also remove energy from the composite. The lower boundary is subjected an insulated boundary condition were $h_2 = 0$ and since the temperature at the lower boundary is close to the ambient temperature, the re-radiation condition is assumed to be negligible as seen in Figure 15. The following parameters in Table 1 were used to solve the model.

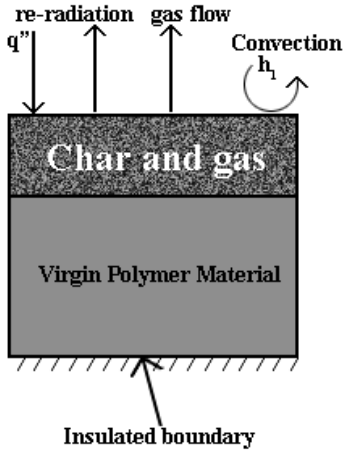

Figure 15: 1-dimensional schematic of boundary conditions

Table 1: Material Property of polyester resin and glass-fiber mat composite

ε	0.9
thickness	0.01 m
$q_0^{"}$	50 kW/m^2
r	0.3, 0.5, 0.7 or 0.9
h_1	10 W/m^{2-}K
h_2	0 W/m^{2-}K
T_a	293 K
T_c	600 K
λ	10^4
k_p	0.3 W/m-K
k_g	0.01 W/mK
ρ_p	900 kg/m^3
$\rho_{g,a}$	1.16 kg/m^3
c_p	2500 J/kgK
c_g	1000 J/kgK
L	10^6 J/kg

Figure 16 and 17 presents these results from this numerical calculation compared with Staggs' results. For the simplicity for calculation, it is assumed in this numerical model that $\hat{\rho}_g$, the dimensionless density of the gas from charring, is incompressible, therefore equal to 1. After calculating the results an immediate conclusion can be seen that the lower the charring ratio, *r*,

the more the numerical model in this paper closely represents Staggs' results. Significant deviation can be seen with r = 0.7 and 0.9, even though at r = 0.3, the results matches almost exactly.

There are a few interesting notes to point out in the presented results. Notice that the mass flux graph, Figure 16, has a two peak characteristic where the first peak has the maximum mass flux value within the first 100 seconds of charring and the second peak is significantly lower in value when compared to the first. Also in Figure 16, it can be reasoned that as the charring ratio increases, the less gas were produced therefore decreasing the maximum mass flux ($\frac{g}{s\,m^2}$). When examining, Figure 17, the results of the surface temperature for all cases seem to match nearly perfectly. It was found that the higher the charring ratio, the lower the surface temperature.

To justify that $\hat{\rho}_g$ is indeed equal to 1, the term to calculate the dimensionless density, derived from Equation (13), was added into the model and the results for mass flux and surface temperature were calculated and compared with the results were $\hat{\rho}_g$ was set equal to 1. Figure 18 and 19 shows these results and they are indeed identical, thus it is a safe assumption that the gas expelled from the charring process is incompressible for this scenario.

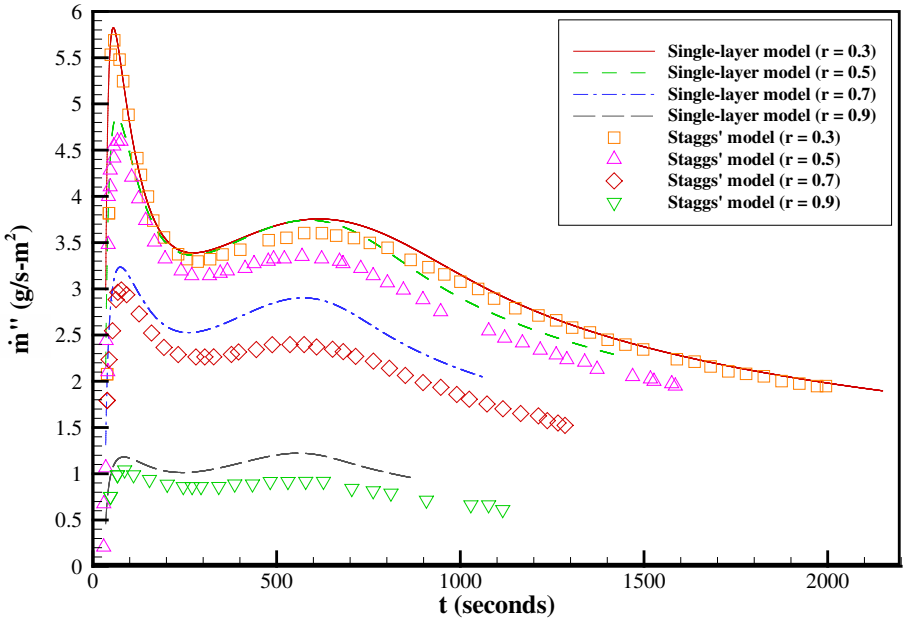

Figure 16: Comparison of mass flux predicted by the single-layer homogeneous model with Staggs' mass flux results

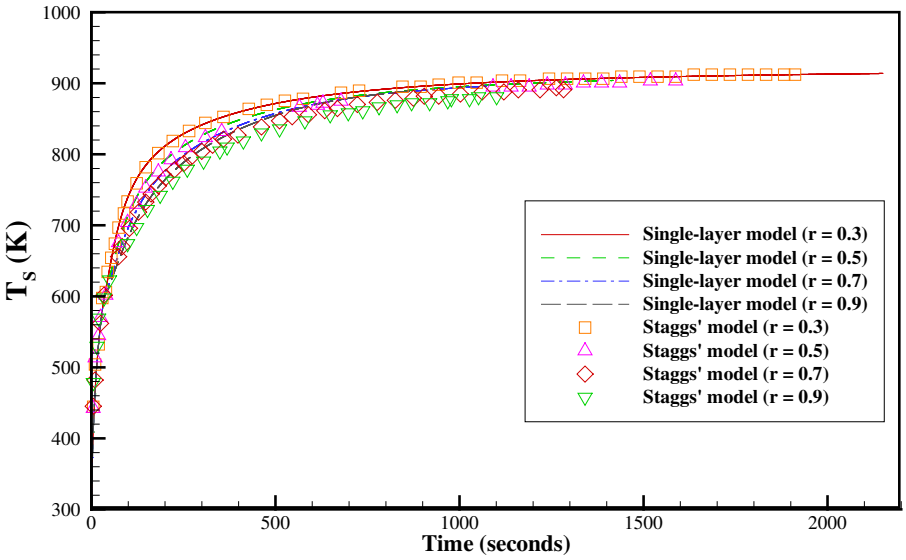

Figure 17: Comparison of surface temperature predicted by the single-layer homogeneous model with Staggs' mass flux results

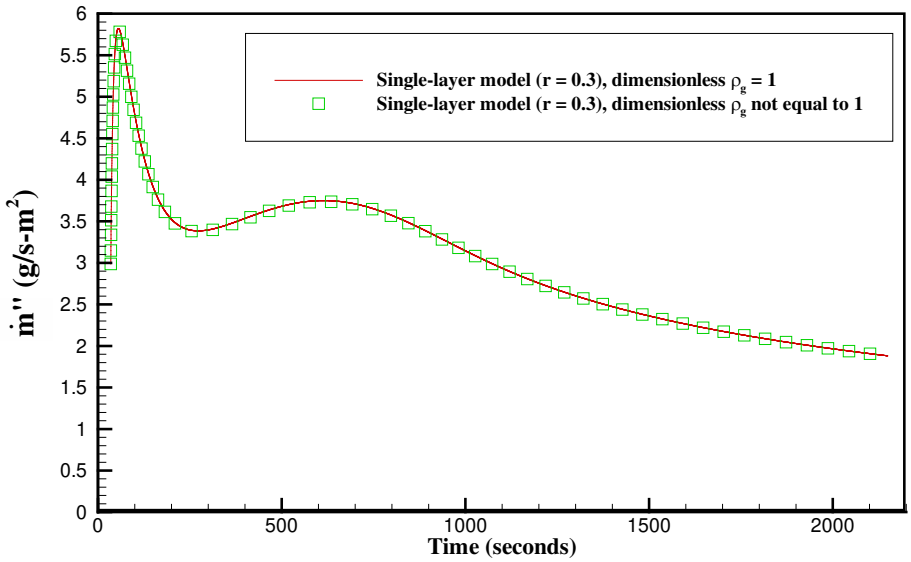

Figure 18: Effect of incompressibility assumption on mass flux results predicted by single-layer homogeneous model

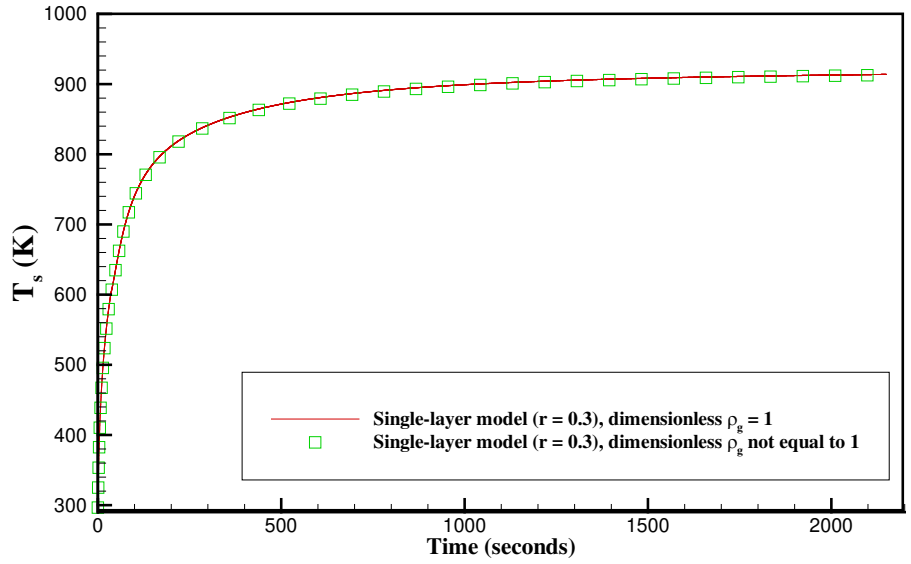

Figure 19: Effect of incompressibility assumption on surface temperature results predicted by single-layer homogeneous model

Homogeneous material zonal model

The zonal-layer numerical model or multiple-layer model is structured like Figure 14 to represent a polyester laminate. In order to validate the zonal-layer model, Staggs' results are utilized again for comparison. To replicate a single layer homogeneous material in the form of a zonal-layer, properties of each layer was kept the same, instead of alternating polyester resin and fiber-glass mat layers, this model has "alternating" polyester resin and polyester resin layers. Staggs' material properties for polyester resin were used to validate the zonal code from Table 1. Due to its excellent accuracy, the results from $r = 0.3$ were used to see the deviations between all three models, Staggs', single-layer, and the zonal-layer.

Results from the zonal-layer model very nearly replicates Staggs' and the single layer code as seen in Figure 20 and 21. There was a slight deviation in the zonal-layer model when compared to the single layer model mainly in maximum value of the first peak. It is also noted that the zonal-layer model finishes its degradation slightly faster than the single layer model. When comparing the surface temperature, the plots match perfectly with almost no noticeable deviation other than the time the degradation ends.

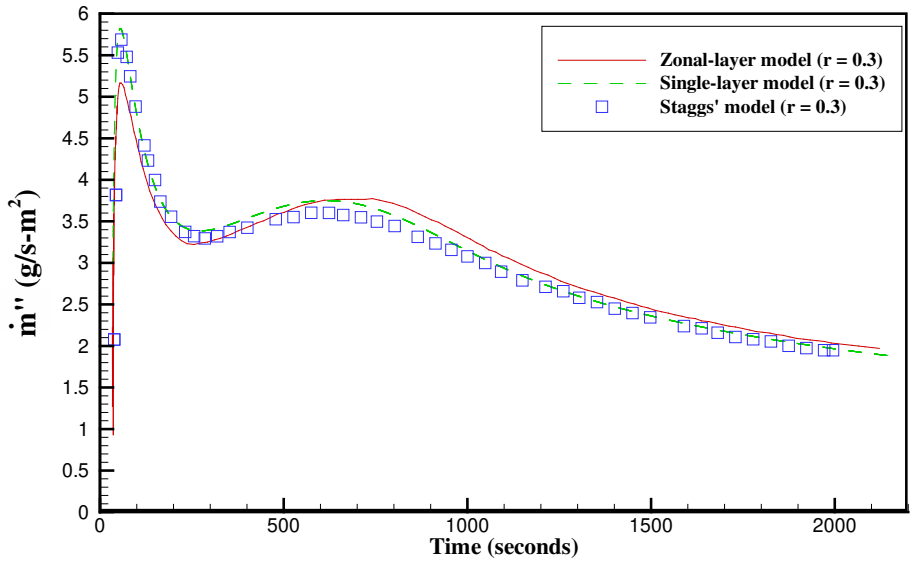

Figure 20: Zonal-layer code validation of mass flux compared with single-layer model and Staggs' model

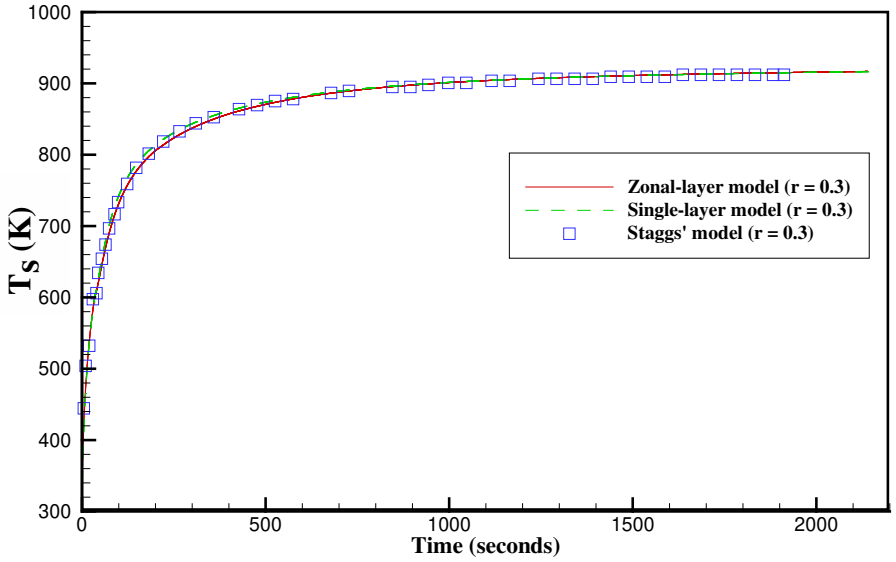

Figure 21: Zonal-layer code validation of surface temperature compared with single-layer model and Staggs' model

Zonal-layer with experimental validation

After validating the zonal-layer model and code, it was desired to see if this numerical model can be applied to experimental data. Figure 22 and 23 displays mass flux and temperature data from two fiberglass reinforced polyester resin laminates with an average thickness of 3.5 mm that were subjected to a cone calorimeter experiment. The two samples are designated C25A and C25B, 'C' for sample of pure polyester resin and fiberglass mats without any additives or fillers. '25' for an external heat flux of 25 kW/m^2, and 'A' and 'B' represents the first and second sample, respectively. Each composite have 4 layers of fiber-glass mat, making a total of 9 layers of alternating polyester resin and fiber-glass mat, it is assumed that each layer have the same thickness, although, in reality this was not the case. I would have been ideal to acquire an microscopic measurement of the thickness in each layer. Figure 24 shows the sample after being exposed to $25kW/m^2$ in the cone calorimeter, note that some char residue is consumed thus showing clean white fiber-glass mat. There were several points that can be made about this experiment and its data. First, in the cone calorimeter, there was a piloted igniter that constantly kept the outgas ignited, this caused another external heat flux from the hydrocarbon flame during combustion. The temperature of the polyester resin and fiberglass laminate was monitored by three thermocouples embedded within each composite, one on top, one on bottom and one as close to the middle as possible. These thermocouples can potentially be a minor cause of heat loss through the wire leads and if the wires are short circuited then the data logger can be reading an incorrect temperature at a different location. An example of incorrect temperature reading due to a short circuit in the thermocouple was seen in Figure 23, the C25A Bottom Temp data plot. Notice how the temperature fails to raise at a rate that represents the trend the other data

plots are exhibiting. That specific thermocouple is most likely short circuited outside the composite and reading an ambient temperature of the room. Due to the insignificance of the erroneous data from the bottom thermocouple of sample C25A, that section of data will be omitted from further discussions and results. Another important observation is that the top thermocouple detached during the degradation due to the lack of structure to hold the sensor in place. If this thermocouple was not attached and happens to have drifted into the flame, then there is a chance that the temperature reading that is logged will be significantly higher than the actual surface temperature.

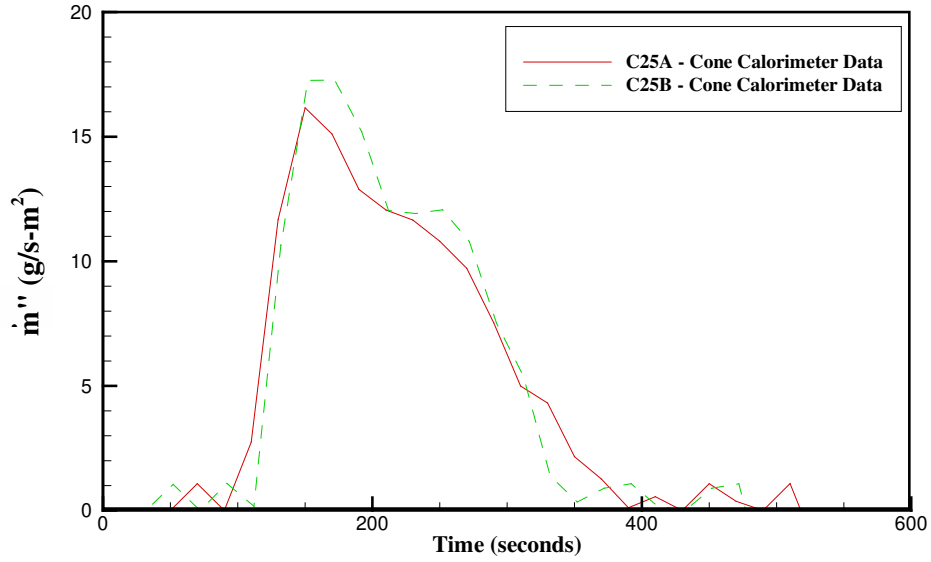

Figure 22: Mass flux data from Cone Calorimeter experiments

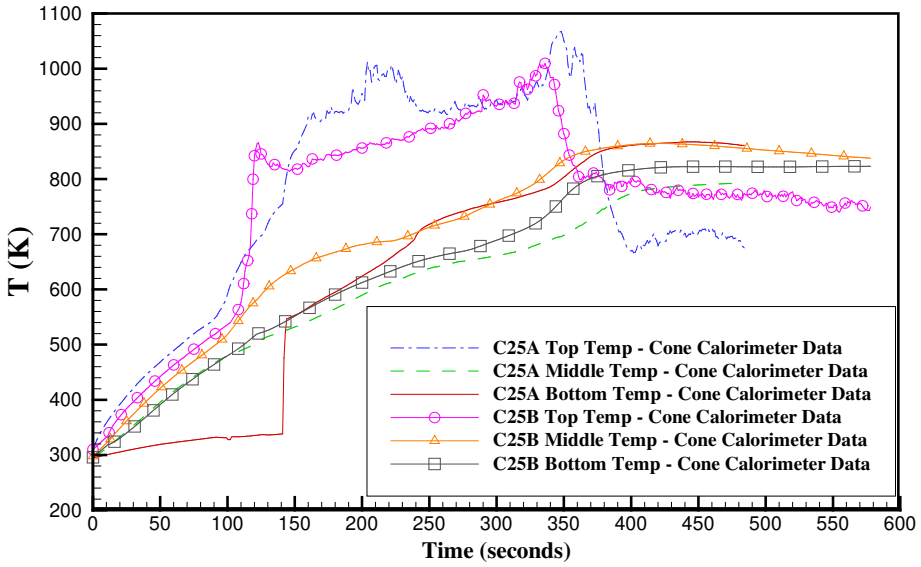

Figure 23: Temperature data from Cone Calorimeter experiments

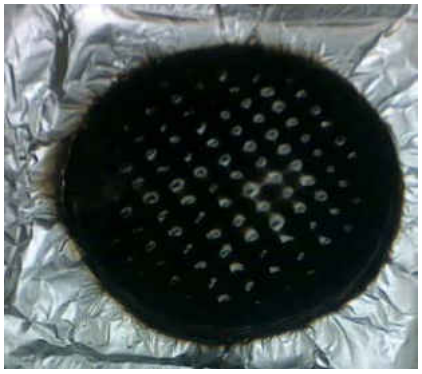

Figure 24: C25A sample after removed from the Cone Calorimeter experiment

Figure 25 to 29 are the results of immediately implementing the zonal-layer material code, assuming homogeneous polyester throughout the entire material, only a few changes were made to the material properties. The critical temperature found in TGA analysis for polyester resin is

close to 523 K and the overall thickness of the material is changed to 3.5 mm oppose to 10 mm from Staggs' simulation. From literature, r = 0.3 is a reasonable assumption to make for polyester resin and will be used in this numerical model although in reality the char residue will be consumed with high heat flux.

The mass flux from the numerical model presented in Figure 25 was not a good representation of the mass flux data from the cone calorimeter. In Figure 25, two numerical results are given, one model of only homogeneous virgin polyester resin, while the second numerical model incorporate interchanging layers of virgin polyester resin layer and glass fiber mats with infused polyester resin layer as depicted in Figure 14. When compared to the cone calorimeter data, the mass flux from both numerical models are lacking in maximum mass flux value and the time it takes to finish degrading is significantly longer. The composite laminate used in the experiment was designed with a volume fraction, V_f, of 0.5. This means 50% of the glass fiber mat and polyester resin layer's volume, illustrated as "Glass mat + Resin" in Figure 14, was glass fiber while the remaining 50% is polyester resin. Glass fiber material has a critical temperature close to 1500 K therefore the polyester resin will degrade much earlier than the glass fiber material. This is evident in Figure 26 for the numerical results with glass fiber mats, notice the sharp decrease in mass flux as the charring front reaches the fiber glass layer due to the lower amount of available polyester resin to degrade. Figure 27 to 29 displays the temperature results compared to the cone calorimeter experimental data. Unfortunately the temperature results were unable to reproduce the experimental data. In Figure 28 it is important to note that the temperature at the middle of the composite display a sudden discontinuity of the graph at about 250 seconds. This marks when the char and polymer interface moving pass the middle point

along the thickness of the material. It was also noted when comparing the result of the predicted model with and without the glass fiber mat that the temperature of the composite with glass fiber mat raises faster.

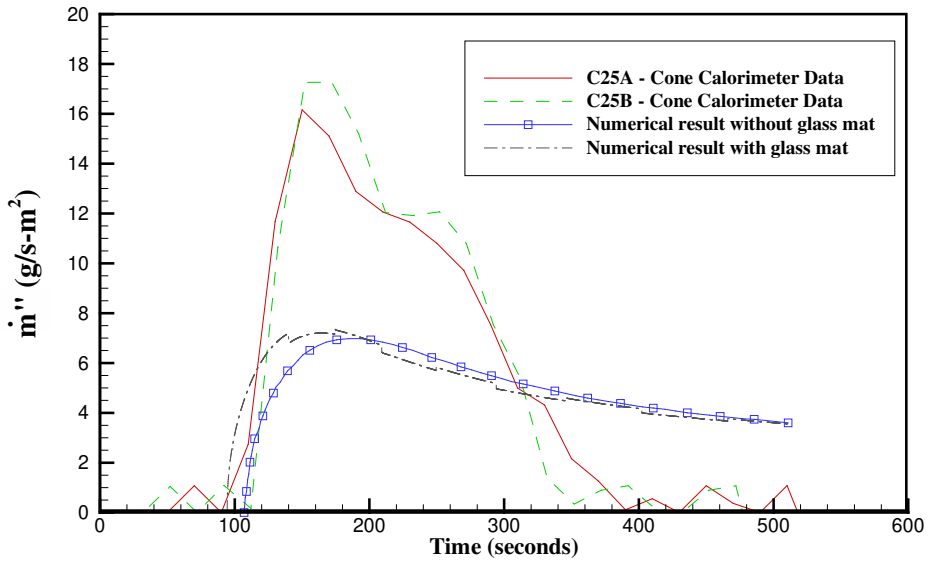

Figure 25: Mass flux predicted by the zonal-layer model with no flame and with or without glass fiber mats, compared with cone calorimeter data

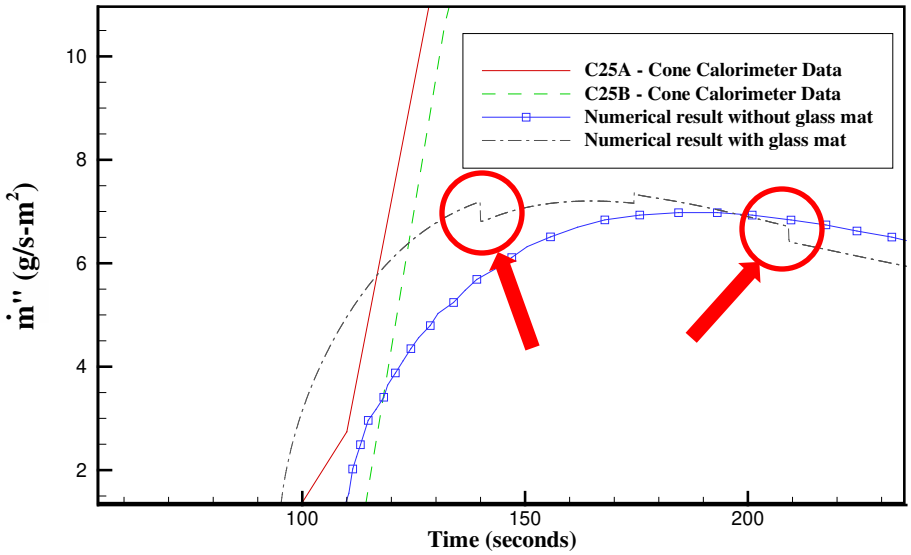

Figure 26: Decrease in mass flux in glass mat layer as indicated by the circle and arrow

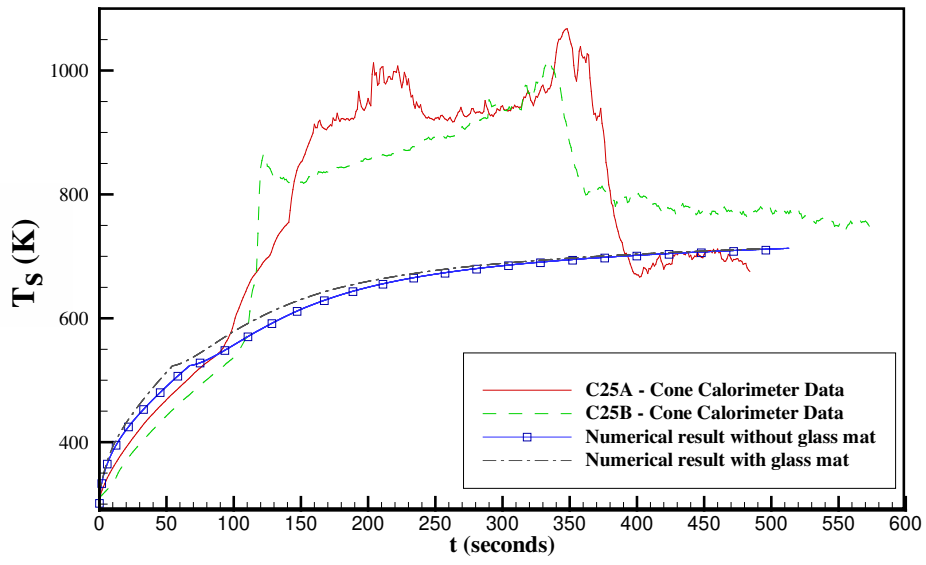

Figure 27: Surface temperature results predicted by the zonal-layer model with no flame and with or without glass fiber mats, compared with cone calorimeter data

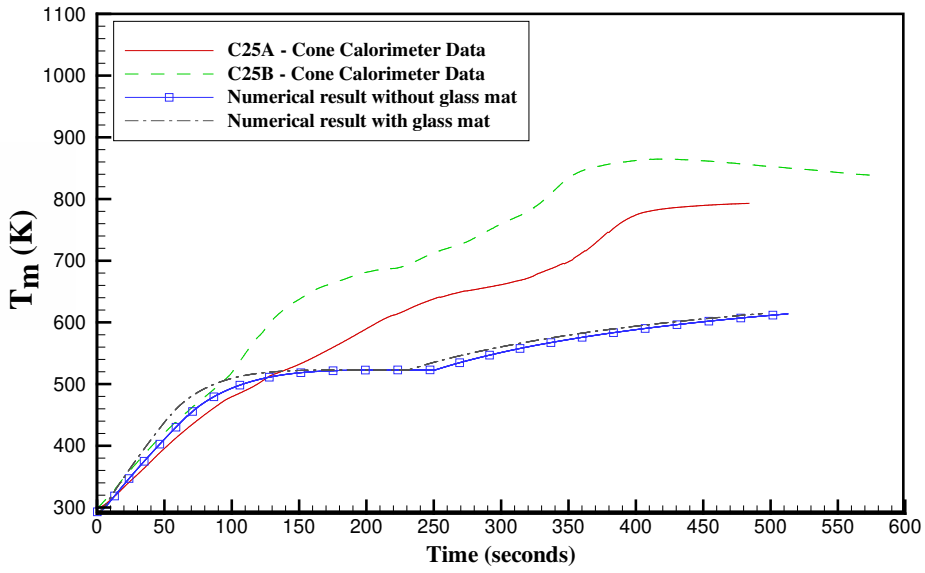

Figure 28: Temperature results at the midpoint of the composite predicted by the zonal-layer model with no flame and with or without glass fiber mats, compared with cone calorimeter data

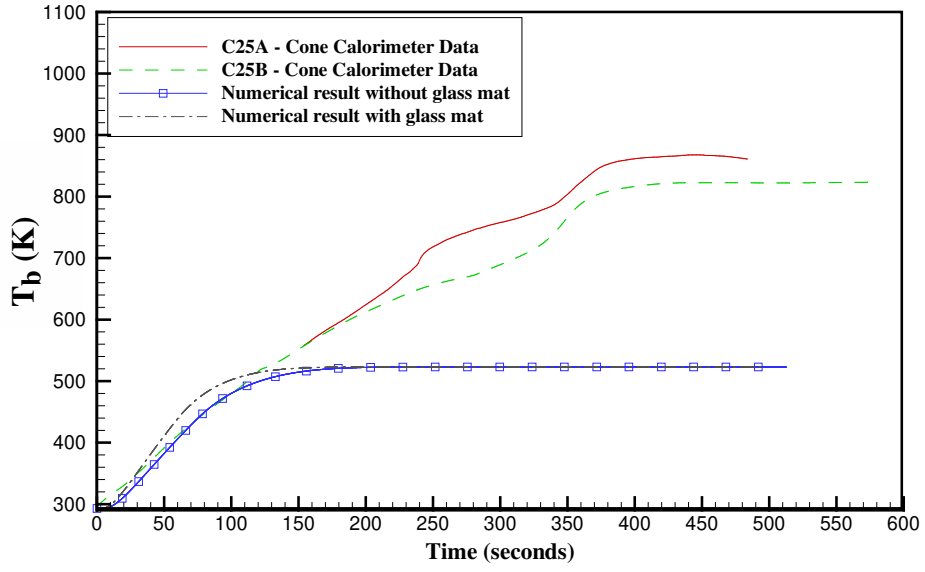

Figure 29: Bottom temperature results predicted by the zonal-layer model with no flame and with or without glass fiber mats, compared with cone calorimeter data

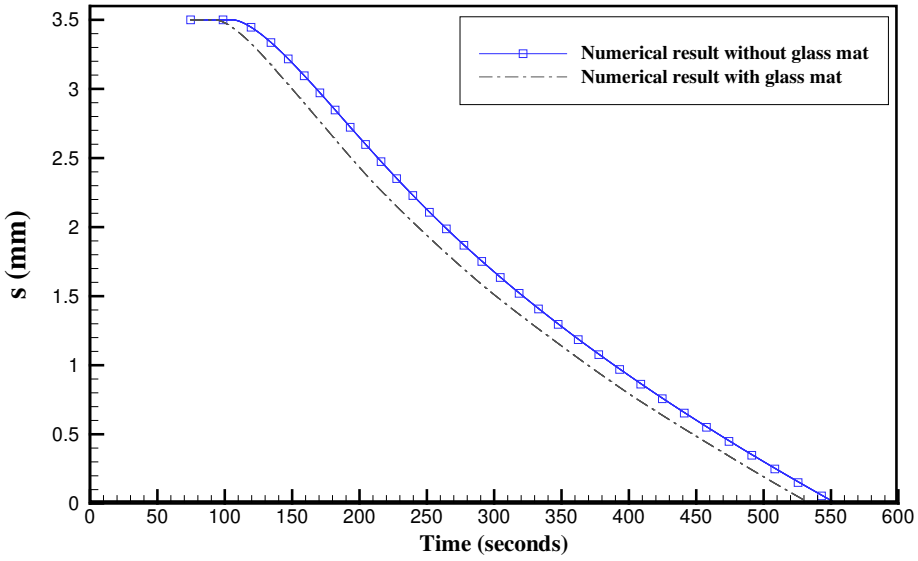

Figure 30: Charring front position predicted by the zonal-layer model with no flame and with or without glass fiber mats

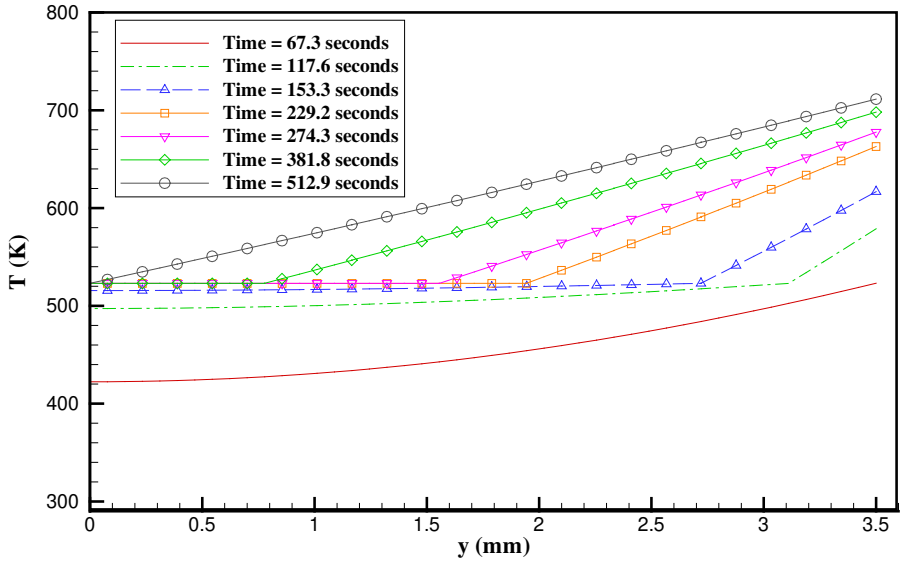

Figure 31: Temperature profile predicted by the zonal-layer model with no flame and without glass fiber mats

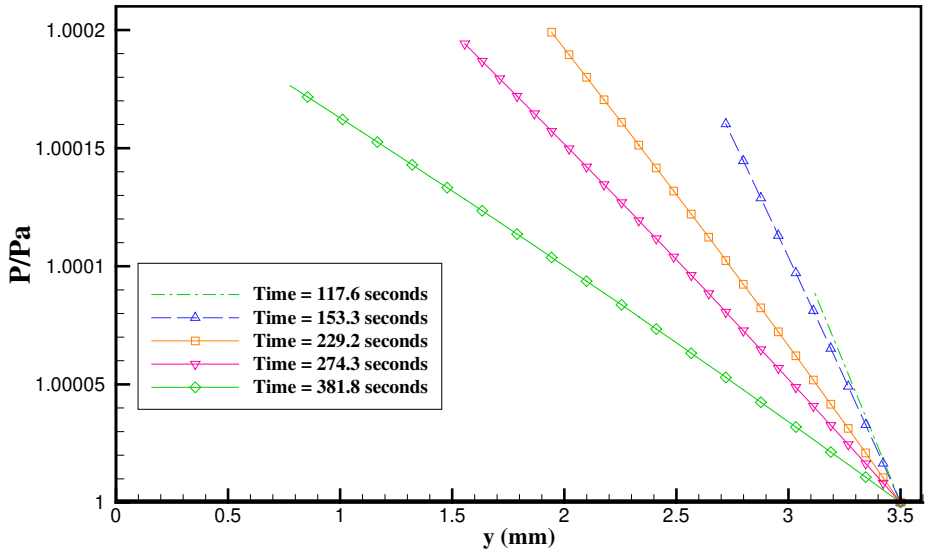

Figure 32: Pressure profile predicted by the zonal-layer model with no flame and without glass fiber mats

Shown in Figure 30 is the position of the char and polymer interface during degradation. This graph can be obtained by integrating numerical results from Figure 25, but in this case, these results were directly outputted by the numerical model. As expected, the char and virgin polymer interface decreases fastest in the beginning of the degradation, this can be correlated to the peak of the mass flux results in Figure 25.

Figure 31 displays the temperature profile within the thickness of the composite, the y-coordinate corresponds to Figure 10. Each line displays the temperature profile at certain times of the numerical model shown in the legend. Figure 32 displays the predicted $\hat{P}$ in the thickness of the charring layer at different times of the numerical model. The gradient of the pressure can be related to the velocity of the degrading gas of the polymer.

An observation that explains the significant deviation in results was the presence of a hydrocarbon flame directly above the sample at the start of material degradation. From previous literature of hydrocarbon flame in a cone calorimeter with polymeric material resulted in an extinction coefficient of 1.4 m^{-1}. To properly model the experimental cone calorimeter data, heat flux from a simulated hydrocarbon flame with an extinction coefficient of 2.0 m^{-1} was used. With a sample diameter of 0.075 m, Equation (23) and (24) resulted in an effective emissivity, ε_f, of 0.1 for the hydrocarbon flame. Soot is a main factor in the extinction coefficient. If a flame produces more soot, then the extinction coefficient is expected to be high. By increasing κ or sample diameter, the emissivity of the flame increases, thus increasing the heat flux received by the composite sample. An example is a flame fueled by polystyrene is found to have a heat release rate of 500 kW with κ equal to 7.5 m^{-1}, while a propane flame with a heat release rate of 110 kW had a κ equal to 0.061 m^{-1} [18]. Heat flux from the flame was simulated to start at the beginning of material degradation. Although the exact flame temperature was not known, it can be assumed that the flame temperature is around 1300 K to 1600 K from the approximate temperature of common hydrocarbon flames. Figure 33 through 36 presents the mass flux and temperature result with an assumed flame temperature of 1300 K and 1600 K.

The sudden addition of a new source of heat flux created a significant jump and sudden jump in mass flux at the beginning of thermal degradation at approximately 100 seconds. It was reasonable to see a significant increase in initial mass flux with a higher flame temperature. The polyester resin will degrade at a much faster rate due to the larger amount of energy incidence into the material. An assumption into why the mass flux plots do not agree could be the fact that the modeling of the hydrocarbon flame is, in fact, impossibly perfect. The flame is modeled to

suddenly appear and bombard the material with its full radiation heat flux capability of 1300 K or 1600 K flame temperature. This was incorrect since the flame, at the beginning, started at the source of ignition and grew to a fully developed turbulent flame in the cone calorimeter. The growth of this flame means the flame temperature will also begin low and increase. This was a reasonable explanation on why a sharp jump in mass flux is not observed for the experimental cone calorimeter data.

One check that has to be made is to see if the amount that was degraded in the experimental cone calorimeter data was the same as the amount degraded in the numerical calculation. By integrating the mass flux plots, the total mass per m^2 area of the degraded material, in the form of gas, is found. Integrating the mass flux of the numerical model, that simulated the cone calorimeter data, resulted in a result of 1676 g/m^2. Cone calorimeter data integration yields 2416 g/m^2 and 2445 g/m^2 for C25A and C25B data respectively. When visually inspecting the sample of cone calorimeter test, it was noticeable that most of the char residue is consumed along with the polyester resin. By dividing 1676 g/m^2 by 0.7, the ratio of degraded gas, the value of 2394 g/m^2 was found which represents the amount of mass per area that was degraded if there was no remaining char residue left. This close match in the adjusted mass result was proof that the char residue itself degrades along with the polymer and was not simulated in this numerical mode.

Figure 34 to 36 displays all the temperature data gathered in the cone calorimeter experiment compared with numerical modeling with the presence of a flame. It's encouraging to see that the temperature before the beginning of degradation was a perfect fit between experimental cone

calorimeter data and numerical results. This gives strong evidence that the material property before the formation of char is a satisfying fit for the polyester resin composite.

The effect of the addition of glass fiber mat on mass flux can be seen in Figure 33, when the char front reaches a fiber-glass mat layer, the mass flux decreases because of the decreased amount of polymer that can char. Adding fiber-glass mats into the composite has a more noticeable effect on the temperature. The general trend present in Figure 34 to 36, when comparing models with fiber-glass mat to models without, was a faster increase in temperature, although a similar steady state temperature was reach for both scenarios.

The top temperature predicted by the model with a flame temperature of 1600 K seems to match the experimental results at first glance but the reader must remember that there was evidence that the top thermocouple broke off from the laminate structure thus reading a higher temperature than the intended surface temperature of the laminate. The bottom temperatures for the numerical model are almost the same for both flame temperature cases, the temperature curve flattens out to approximately 523 K, which corresponds to the critical temperature. This was due to the criteria of degradation specified in the numerical model. The charring front is fixed at 523 K, thus preventing the virgin polymer material from ever exceeding the defined critical temperature. In the experimental case, the bottom temperature does not exhibit the same behavior as the numerical model. This was expected because the char residue itself degrades and the charring process was not at a constant 523 K but in fact the charring process starts around 500 K and was considered fully degraded at 700 K. The middle temperature was read by a thermocouple embedded approximately in the middle of the entire composite. This location is

ideal for comparison with the numerical model because it was not affected by the issues present in the top thermocouple and issues present in the bottom numerically calculated temperature. When comparing the experimental and numerical data for the middle temperature seen in Figure 35, it's noticed that the data with a flame temperature of 1300 K is a very strong fit with the C25A cone calorimeter data which further backs the belief that the flame temperature is close to 1300 K instead of 1600 K. Also notice that the experimental data continues for a longer duration and temperature continues to rise when compared to the numerical results. An explanation returns to the previous argument that char degradation begins at 500 K and finishes degradation at 700 K and that the char residue continues to burn.

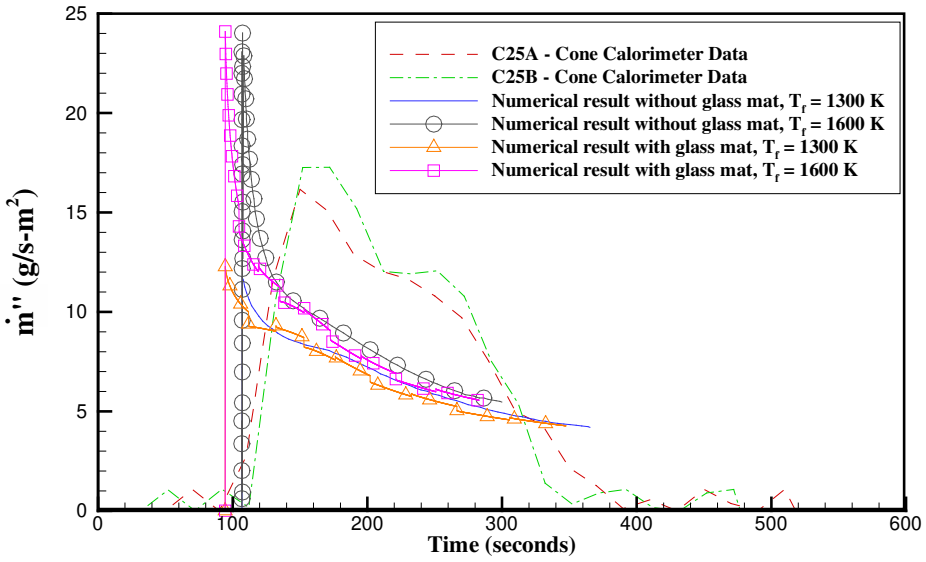

Figure 33: Mass flux predicted by the zonal-layer model with flame and with or without glass fiber mats, compared with cone calorimeter data

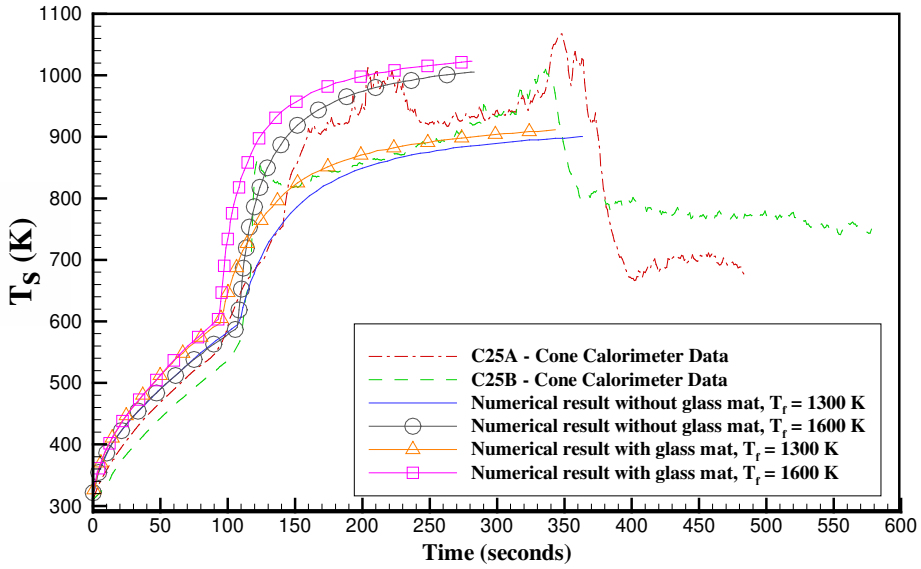

Figure 34: Surface temperature results predicted by the zonal-layer model with flame and with or without glass fiber mats, compared with cone calorimeter data

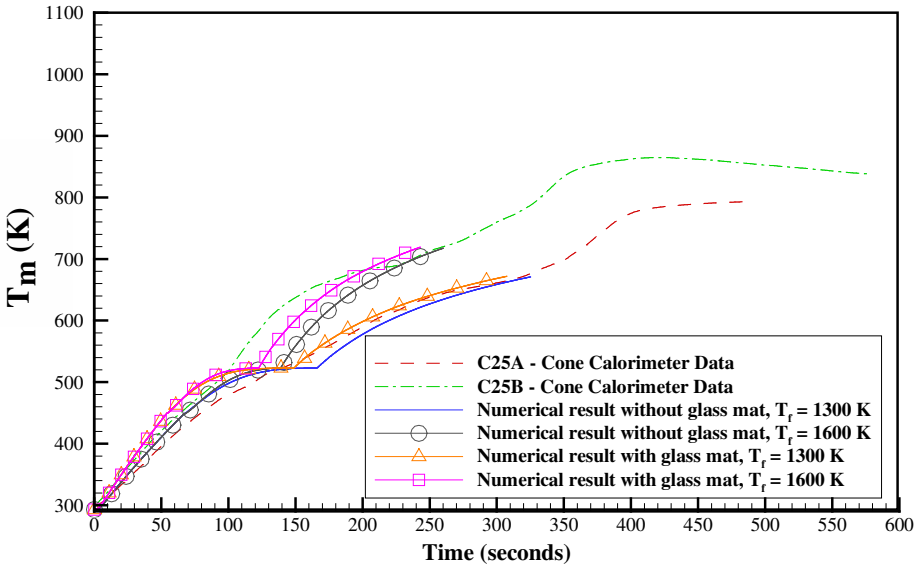

Figure 35: Temperature results at the midpoint of the composite predicted by the zonal-layer model with flame and with or without glass fiber mats, compared with cone calorimeter data

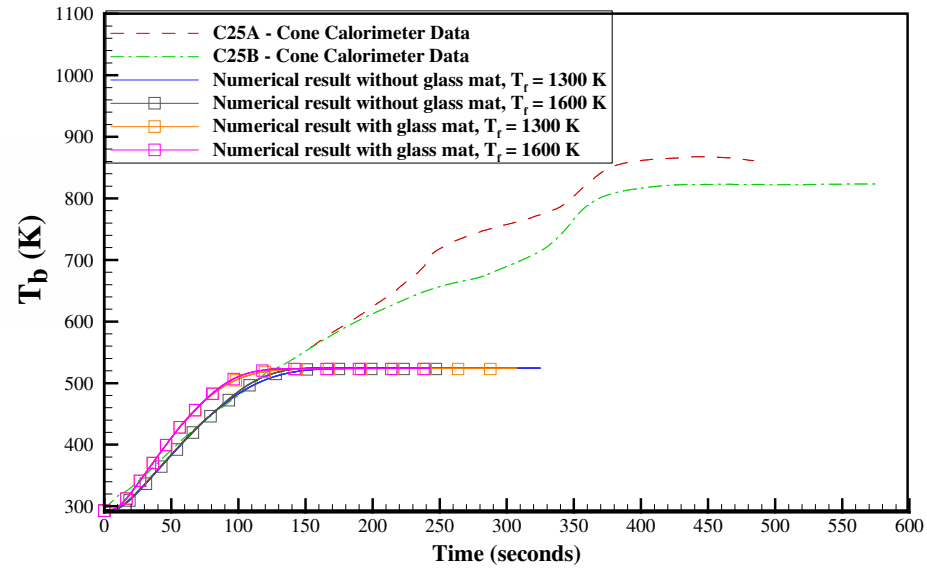

Figure 36: Bottom temperature results predicted by the zonal-layer model with flame and with or without glass fiber mats, compared with cone calorimeter data

The char and virgin polymer interface position is shown in Figure 37. An expected trend here is the presence of a higher flame temperature results in a more rapidly decreasing interface position when compared to a model with flame temperature of 1300 K. Another trend can be seen when comparing the numerical result without glass fiber mat to the result with the glass fiber mat was the results with the glass mat will take a little longer to fully degrade.

Shown in Figures 38 and 39 is the temperature profile results along the thickness of the composite. The y-coordinate in Figure 38 represents the coordinate system in Figure 10. Figure 40 and 41 presents $\hat{P}$ along the thickness of the charring layer. It was interesting to note that the magnitude of the pressure within the charring layer of the model with flame temperature of 1600

K, was higher than the model with a flame temperature of 1300 K. This is due to the significantly higher mass flux as seen from Figure 33.

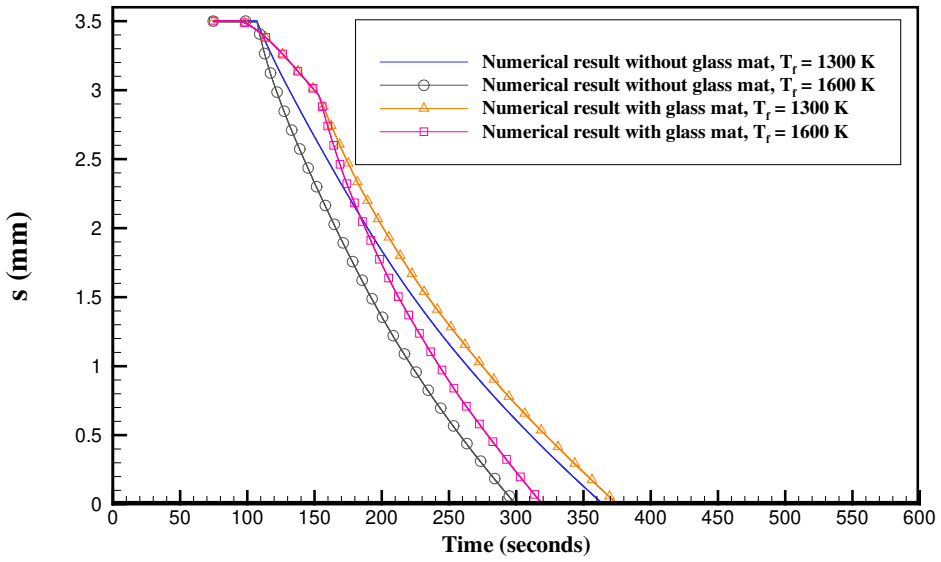

Figure 37: Charring front position predicted by the zonal-layer model with flame and with or without glass fiber mats

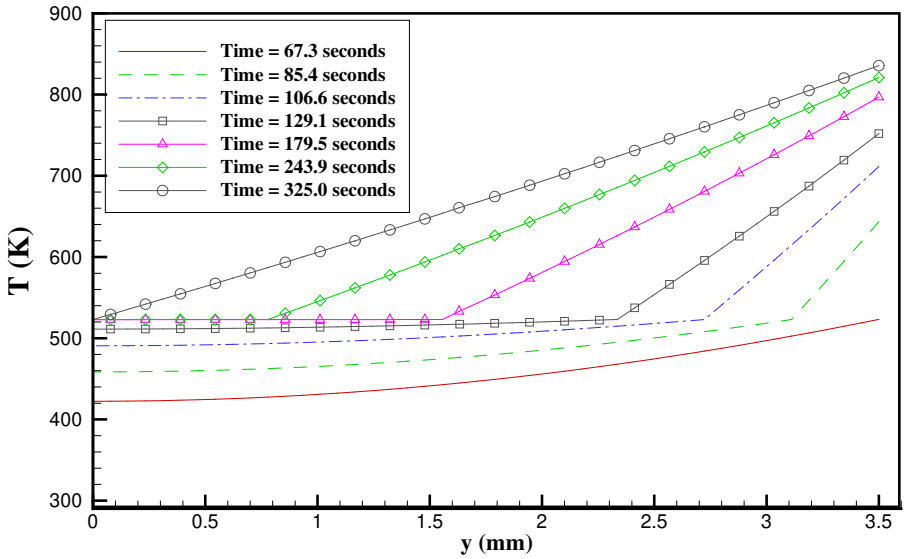

Figure 38: Temperature profile predicted by the zonal-layer model with flame, T_f = 1300 K, and without glass fiber mats

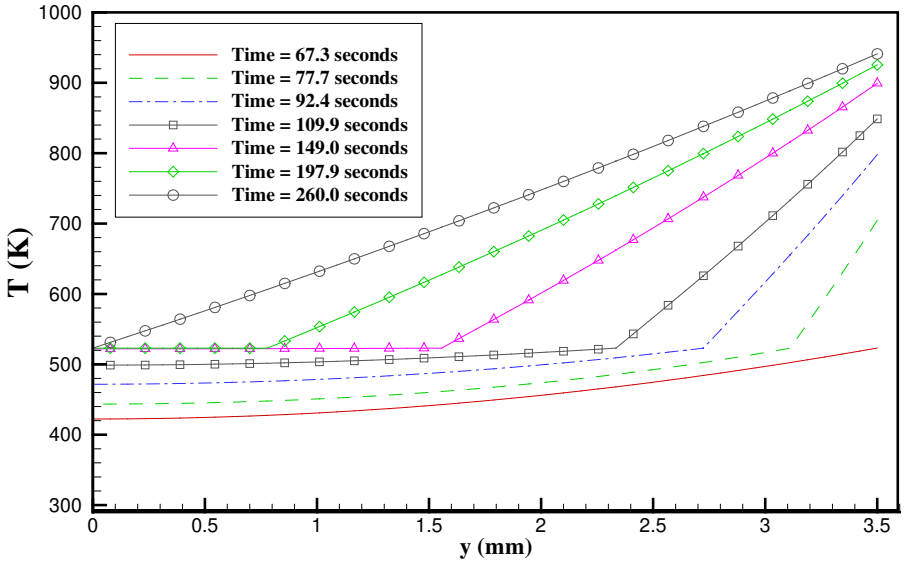

Figure 39: Temperature profile predicted by the zonal-layer model with flame, T_f = 1600 K and without glass fiber mats

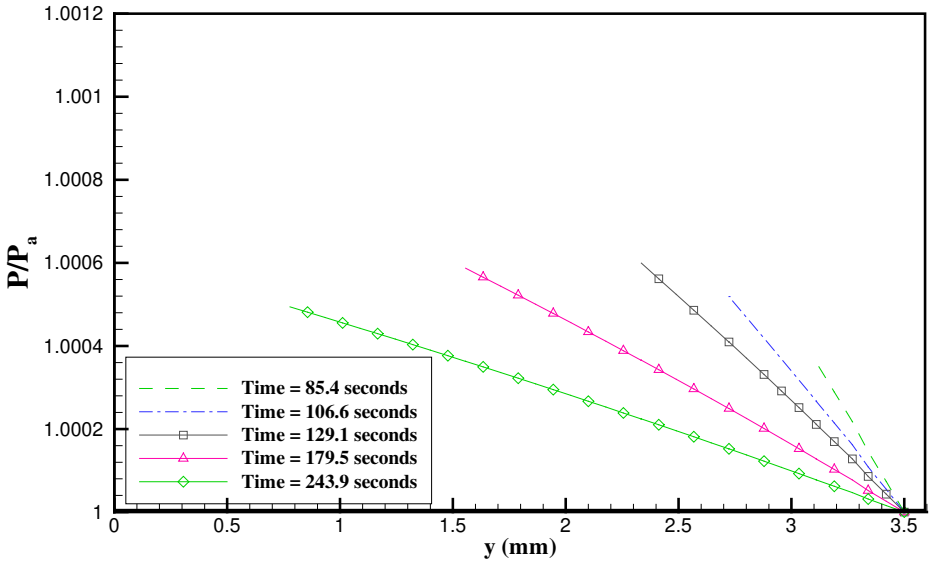

Figure 40: Pressure profile predicted by the zonal-layer model with flame, T_f = 1300 K, and without glass fiber mats

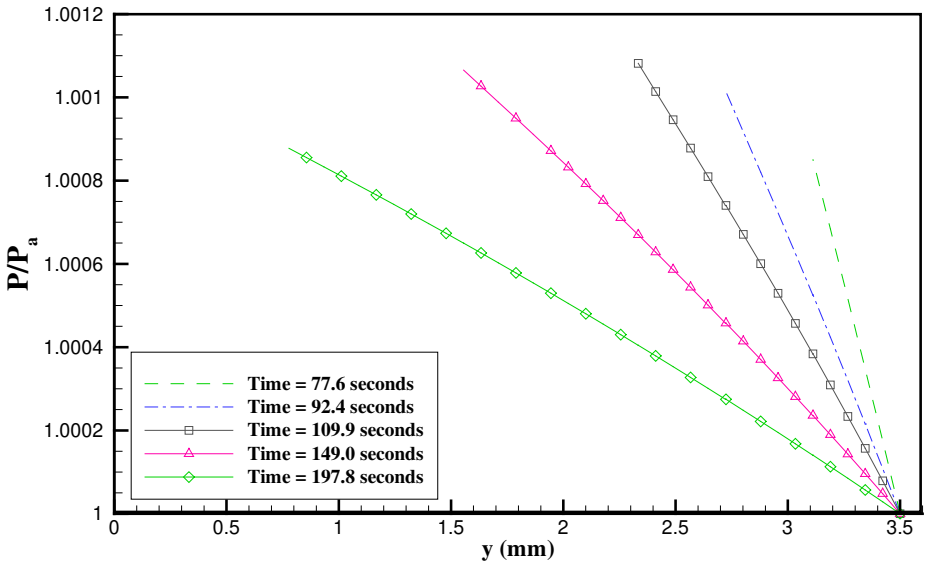

Figure 41: Pressure profile predicted by the zonal-layer model with flame, T_f = 1600 K, and without glass fiber mats

Grid Analysis

There is a chance that the incorrect sizing of the grid of nodes used in the numerical model was a cause of error. To validate this numerical model of homogeneous material with a flame temperature at 1600 K was computed with various node counts. Figure 13 displays the schematic of the nodes for the zonal-layer model were N is equal to 5, 7, and 9 for the grid analysis. All results presented before this section is computed with N = 5, but it is seen that increasing the node count resulted in absolutely no visible deviation.

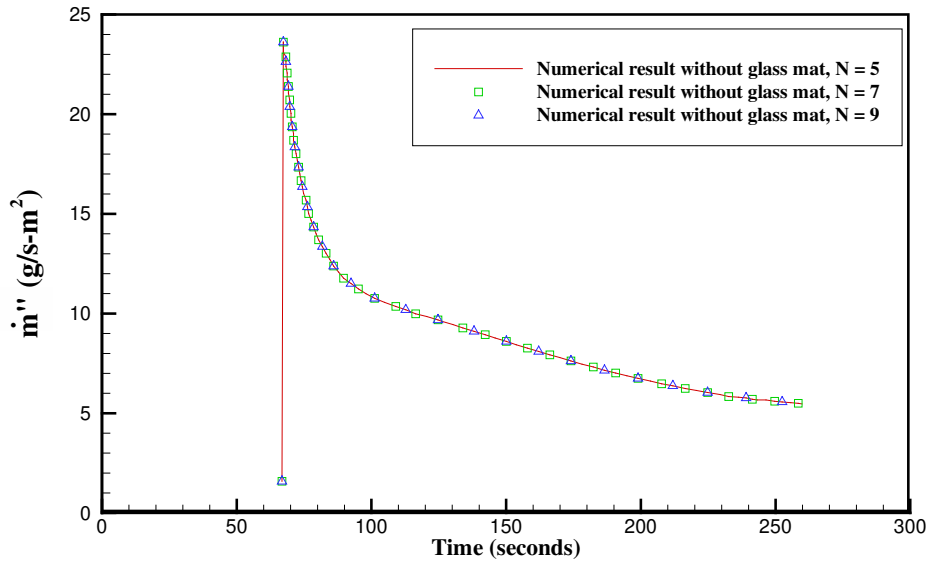

Figure 42: Grid analysis of mass flux predicted by the zonal-layer model with flame, T_f = 1600 K and without glass fiber mats where N is defined in Figure 13

CHAPTER FOUR: CONCLUSION

The development of the numerical model was for comparison with a glass-fiber reinforced polyester resin composite in a cone calorimeter. Mass flux comparison deviates significantly but temperature data and calculated results from the middle from the composite matches well. Improvements can be made in future cone calorimeter experiment by embedding more temperature sensors along the thickness of the composite and improving temperature reading methods for the degrading structure. Experimental improvements will provide better validation results of the numerical model. Flame temperature data and soot concentration data from the cone calorimeter experiment will also provide a better simulation of flame radiation heat flux.

Even though the temperature data from the middle thermocouple of the experiment matches the calculated results from the numerical model, the resulted temperature of the bottom of the composite is found to be a very poor representation of experimental data. The bottom of the composite is the more significant result desired because it provides the information of when the entire composite is fully degraded, resulting in absolutely no structure. Since the char and polymer interface criteria is set to a constant temperature, this causes a significant problem in replicating reality, since the charring process is in fact, not a single point fixed at a single critical temperature, but a range between 400 K to 700 K. It is ideal to use the Arrhenius rate of reaction to calculate the mass flux, instead of the latent heat of the polymer so that the char and polymer interface is not fixed at a very specific temperature. It is also significant that the char residue will degrade when exposed to a high heat flux which is expected to affect the mass flux results.

With the knowledge of the flame emissivity and temperature, the thermal behavior of any composite can be simulated with this numerical model. This is truly a significant tool in understanding the behavior of composite properties under thermally degrading conditions. By modifying matrix properties, fiber properties or adding additives to the composite, the researchers can possibly improve results to combat the degradation of polymer composites. To accomplish this task in a time and costly manner, this numerical model was developed.

LIST OF REFERENCES

[1] Gerrard J., Milind K., Is European end-of-life vehicle legislation living up to expectations? Assessing the impact of the ELV Directive on 'green' innovation and vehicle recovery. Journal of Cleaner Production, vol. 15, pp. 17-27, 2007.

[2] P.K. Mallick. "Fiber-reinforced composites: materials, manufacturing and design. Third edition". CRC Press., 2008.

[3] Irvin Glassman, Richard A. Yetter. "Combustion. Fourth edition". Academic Press., 2008.

[4] Robert Siegel and John Howell, "Thermal Radiation Heat Transfer, 4th edition". Taylor & Francis, 2002.

[5] Joshua L. Jurs. Development and testing of flame retardant additives and polymers. FAA. U.S. Department of Transportation. 2007.

[6] Schartel B., Hull T.R., Development of fire-retarded materials – Interpretation of cone calorimeter data, Fire and Materials, vol. 31, pp. 327-354, 2007.

[7] Bamford C.H., Crank J., Malan D.H., The combustion of wood. Part 1. Mathematical Proceedings of the Cambridge Philosophical Society, vol. 42 pp. 166-182, 1946.

[8] Henderson J.B., Wiebelt J.A., Tant M.R., A Model for the Thermal Response of Polymer Composite Materials with Experimental Verification. *Journal of Composite Materials*, vol. 19, pp. 579-595, 1985.

[9] Staggs J.E.J., Heat and mass transport in developing chars. *Polymer Degradation and Stability*, vol. 82, pp. 297-307, 2003.

[10] Krysl P., Ramroth W.T., Stewart L.K., Asaro R.J., Finite element modeling of fibre reinforced polymer sandwich panels exposed to heat. *International journal for numerical methods in engineering*, vol. 61 pp. 49-68, 2004.

[11] Quintiere J.G., A theoretical basis for flammability properties. Fire and materials, vol. 30 pp. 175-214, 2006.

[12] Jiang F., Flame radiation from polymer fires. Fire safety journal, vol. 30 pp. 383-395, 1998.

[13] Brian T. Rhodes., "Burning rate and flame heat flux for PMMA in the cone calorimeter". U.S. Department of Commerce, 1994.

[14] Farkas E., Meszena Z.G., Toldy A., Matko S., Marosfoi B.B., Marosi Gy., Modelling of transport processes in a developing char. *Polymer degradation and stability*, vol 93 pp.1205-1213, 2008.

[15] Staggs J.E.J., Estimating the thermal conductivity of chars and porous residues using thermal resistor networks. *Fire Safety Journal*, vol. 37 pp. 107-119, 2002.

[16] Landau H.G., Heat conduction in a melting solid. Quarterly of Applied Mathematics, vol. 8 pp. 81-94, 1950.

[17] Looyeh M.R.E., Bettess P., A finite element model for the fire-performance of GRP panels including variable thermal properties. *Finite Element in Analysis and Design*, vol. 30, pp. 313-324, 1998.

[18] Putori, Jr., Anthony, Design Parameters for Stack-mounted Light Extinction Measurement Device. *NIST*.